JOURNAL OF GEOPHYSICAL RESEARCH: ATMOSPHERES, VOL. 118, 12,766–12,783, doi:10.1002/2013JD020577, 2013

Using FTIR measurements of stratospheric composition to identify midlatitude polar vortex intrusions over Toronto

C. Whaley,[1] K. Strong,[1] C. Adams,[1,2] A. E. Bourassa,[2] W. H. Daffer,[3] D. A. Degenstein,[2] H. Fast,[4] P. F. Fogal,[4] G. L. Manney,[5,6] R. L. Mittermeier,[4] B. Pavlovic,[1,7] and A. Wiacek[8]

Received 18 July 2013; revised 28 October 2013; accepted 8 November 2013; published 22 November 2013.

[1] Using 11 years of trace gas measurements made at the University of Toronto Atmospheric Observatory (43.66°N, 79.40°W) and Environment Canada's Centre for Atmospheric Research Experiments (44.23°N, 79.78°W), along with derived meteorological products, we identify a number of polar intrusion events, which are excursions of the polar vortex or filaments from the polar vortex extending down to midlatitudes. These events are characterized by enhanced stratospheric columns (12–50 km) of hydrogen fluoride (HF), by diminished stratospheric columns of nitrous oxide (N_2O), and by a scaled potential vorticity above $1.2 \times 10^{-4}s^{-1}$. The events comprise 16% of winter/spring (November to April inclusive) Fourier transform infrared (FTIR) spectroscopic measurements from January 2002 to March 2013, and we find at least two events per year. The events are corroborated by Modèle Isentrope du transport Méso-échelle de l'Ozone Stratosphérique par Advection, Modern-Era Retrospective Analysis for Research and Applications potential vorticity maps, and Global Modeling Initiative N_2O maps. During polar intrusion events, the stratospheric ozone (O_3) columns over Toronto are usually greater than when there is no event. Our O_3 measurements agree with the Optical Spectrograph and Infrared Imaging System satellite instrument and are further verified with the Earth Probe Total Ozone Mapping Spectrometer and Ozone Monitoring Instrument satellite observations. We find six cases out of 53 for which chemical O_3 depletion within the polar vortex led to a reduction in stratospheric O_3 columns over Toronto. We have thus identified a dynamical cause for most of the winter/spring variability of stratospheric trace gas columns observed at our midlatitude site. While there have been a number of prior polar intrusion studies, this is the first study to report in the context of 11 years of ground-based FTIR column measurements, providing insight into the frequency of midlatitude polar vortex intrusions and observations of upper stratospheric (25–50 km) intrusions. It is also the first to present HF measurements during multiple polar intrusions, which provided an excellent tracer for their identification.

Citation: Whaley, C., et al. (2013), Using FTIR measurements of stratospheric composition to identify midlatitude polar vortex intrusions over Toronto, *J. Geophys. Res. Atmos.*, *118*, 12,766–12,783, doi:10.1002/2013JD020577.

1. Introduction

[2] The stratospheric polar vortex is a large low-pressure system that persists over the winter pole for many months, characterized by low temperatures, high potential vorticity (PV), and high winds near its boundary. The descent of air within the polar vortex and its relative isolation result in a distinctive chemical composition; hydrogen chloride (HCl), hydrogen fluoride (HF), and ozone (O_3) total and stratospheric columns tend to be enhanced because when stratospheric gases descend in altitude, they main-

[1]Department of Physics, University of Toronto, Toronto, Ontario, Canada.
[2]Department of Physics and Engineering Physics, University of Saskatchewan, Saskatoon, Saskatchewan, Canada.
[3]Jet Propulsion Laboratory, California Institute of Technology, Pasadena, California, USA.
[4]Air Quality Research Division, Atmospheric Science and Technology Directorate, Science and Technology Branch, Environment Canada, Toronto, Ontario, Canada.
[5]NorthWest Research Associates, Socorro, New Mexico, USA.
[6]Department of Physics, New Mexico Institute of Mining and Technology, Socorro, New Mexico, USA.
[7]Department of Physics, University of Guelph, Guelph, Ontario, Canada.
[8]Environmental Science, Saint Mary's University, Halifax, Nova Scotia, Canada.

Corresponding author: C. Whaley, Whaley, Department of Physics, University of Toronto, 60 St. George Street, Toronto, ON M5S 1A7, Canada. (cwhaley@atmosp.physics.utoronto.ca)

2169-897X/13/10.1002/2013JD020577

tain their mixing ratio but number densities increase. O_3 columns in particular are increased (in the absence of chemical O_3 loss) during winter because of poleward transport from the tropics and then descent via the Brewer-Dobson circulation. Similarly, the descent of long-lived tropospheric gases like nitrous oxide (N_2O, which is destroyed in the stratosphere) results in diminished columns of N_2O in the polar vortex [*Schoeberl et al.*, 1992, 1995; *Brasseur et al.*, 1999].

[3] The northern polar vortex typically extends down to about 65°–68°N in latitude when centered near the North Pole, and its edge has been defined in a number of ways: using PV gradients and wind speeds [e.g., *Nash et al.*, 1996], the Q-diagnostic method [e.g., *Harvey et al.*, 2002], or scaled PV [e.g., *Manney et al.*, 2007]. In the spring, when the vortex breaks up, parts or fragments of a highly distorted vortex can extend to much lower latitudes [*Waugh et al.*, 1994; *Orsolini*, 1995; *Hauchecorne et al.*, 2002]. Excursions of the polar vortex to midlatitudes have been observed and modeled [*Godin et al.*, 2002; *Marchand et al.*, 2003; *Konopka et al.*, 2003; *Durry and Hauchecorne*, 2005; *Duchatelet et al.*, 2009], as have filaments breaking off the polar vortex and extending to the midlatitudes [*Leovy et al.*, 1985; *Andrews et al.*, 1987; *Pierce and Fairlie*, 1993; *Manney et al.*, 1998, 2000; *Newman et al.*, 1996; *Orsolini et al.*, 1998; *Godin et al.*, 2002; *Hauchecorne et al.*, 2002; *Marchand et al.*, 2003; *Millard et al.*, 2003; *Tripathi et al.*, 2006]. Filaments are formed when the vortex edge is deformed by meridional winds induced by planetary Rossby waves breaking [*McIntyre and Palmer*, 1984; *Waugh et al.*, 1994] and subtropical anticyclones [*Pierce and Fairlie*, 1993]. The filaments are stretched out by the meridional gradient of the zonal wind over the course of a few days [*Pierce and Fairlie*, 1993; *Marchand et al.*, 2003].

[4] The previous studies of polar intrusion events mentioned above used measurements of O_3, CH_4, N_2O, HCl, H_2O, CO_2, COF_2, and CFCs from lidars, ozonesondes, aircraft-borne photometry and spectroscopy, ground-based spectroscopy, and balloon-borne in situ instruments, as well as reverse domain-filling trajectory calculations [e.g., *Sutton et al.*, 1994; *Schoeberl and Newman*, 1995; *Manney et al.*, 1998, 2000], and 3-D chemical transport models (CTMs) such as the Single Layer Isentropic Model of Chemistry And Transport, the Chemical Lagrangian Model of the Stratosphere, and the Modèle Isentrope du transport Méso-échelle de l'Ozone Stratosphérique par Advection (MIMOSA) to detect and model polar intrusion events. There have been several studies of polar intrusion events observed over Europe [*Orsolini et al.*, 1997, 1998; *Godin et al.*, 2002; *Durry and Hauchecorne*, 2005], but only a few over North America (and Hawaii) [*Newman et al.*, 1996; *Manney et al.*, 1998; *Tripathi et al.*, 2006].

[5] Polar intrusion events can have varying, but significant, effects on midlatitude O_3 columns. When the vortex is cold and stable, conditions are favorable for chemical O_3 depletion but are unfavorable for filamentation, and thus to transport to midlatitudes [*Hauchecorne et al.*, 2002; *Millard et al.*, 2003]. Conversely, when a stratospheric warming occurs, the polar vortex is more likely to break up and extend to midlatitudes [*Waugh et al.*, 1994; *Hauchecorne et al.*, 2002]. It has been reported that up to 50% of midlatitude O_3 volume mixing ratio (VMR) decreases at 475 K can be accounted for by intrusions of O_3-poor polar air to midlatitudes [*Marchand et al.*, 2003; *Millard et al.*, 2003]. However, increases in midlatitude O_3 due to polar vortex intrusions have also been reported [e.g., *Godin et al.*, 2002; *Tripathi et al.*, 2006].

[6] The goals of the present study are to use long-term measurements to estimate how often polar intrusion events occur over the Toronto region (a large metropolitan area of about six million people) and to determine whether these polar intrusion events can explain some of the variability in the time series of trace gases observed at this midlatitude location. This study is the first to report polar intrusion events over southern Canada, using long-term ground-based measurements of stratospheric partial columns (12–50 km) of HF and N_2O obtained by Fourier transform infrared (FTIR) spectroscopy to identify their occurrence. Given that there was unprecedented Arctic O_3 loss in spring 2011 [*Balis et al.*, 2011; *Manney et al.*, 2011; *Adams et al.*, 2012; *Lindenmaier et al.*, 2012], we are also interested in determining whether O_3 columns above Toronto were diminished during 2011 polar intrusion events.

[7] HF is an excellent dynamical tracer for the polar vortex because it has a long lifetime, and as mentioned previously, it has a greater density inside the polar vortex [*Chipperfield et al.*, 1997; *Toon et al.*, 1999; *Mellqvist et al.*, 2002; *Coffey et al.*, 2008]. Therefore, we examine 11 years of Toronto FTIR data (January 2002 to March 2013), looking for outliers of HF as an indicator of polar air. Polar intrusions are then either confirmed or discounted as the source of the outliers using scaled potential vorticity, models, and satellite observations, which provide more spatial coverage, showing the polar vortex structure at the time of the HF outlier.

[8] This paper is organized as follows. The next section briefly describes our measurements. Section 3 describes the MIMOSA model and the Modern-Era Retrospective Analysis for Research and Applications (MERRA) data assimilation system from which PV has been used to confirm the occurrence of polar intrusion events. The Global Modeling Initiative (GMI) CTM and derived meteorological products (DMPs) are also described in this section. This is followed by a discussion of our results (section 4) and conclusions (section 5).

2. Measurements

2.1. TAO FTIR Spectrometer

[9] The primary measurements used in this study are made by a ground-based, high-resolution (0.004 cm^{-1}) Bomem DA8 FTIR spectrometer at the University of Toronto Atmospheric Observatory (TAO), 43.66°N, 79.4°W, 174 meters above sea level (masl) [*Wiacek et al.*, 2007]. The TAO FTIR spectrometer was installed in late 2001 and has been operational for daily measurements, weather permitting, since May 2002. TAO became a site in the Network for Detection of Atmospheric Composition Change (NDACC) in 2004. We retrieve total and partial column amounts of HCl, HF, O_3, and N_2O using the optimal estimation method [*Rodgers*, 2000] implemented with the SFIT2 [*Rinsland et al.*, 1998; *Pougatchev et al.*, 1995] v3.94 algorithm and the High-resolution Transmission molecular absorption database 2008 spectral line list [*Rothman et al.*, 2009]. Temperature and pressure profiles are obtained from

Table 1. TAO and CARE FTIR Retrieval Parameters[a]

Species	Microwindow(s) (cm^{-1})	Interfering Species	SNR	$\mathbf{S}_a$	DOFS	Partial Column Errors
HF	4038.86–4039.05	H_2O	250	20%	1.2/1.2	3.0%/1.1%
HCl	2727.73–2727.83	O_3, HDO	300	10–40%	3.5/3.2	3.5%/2.0%
	2775.70–2775.80	N_2O, O_3				
	2925.80–2926.00	NO_2, O_3, CH_4				
N_2O	2481.30–2482.60	CO_2, CH_4, O_3, H_2O, HDO	100	20%	3.7/1.8	9.0%/1.8%
	2526.40–2528.20	CO_2, CH_4, O_3, H_2O, HDO				
	2537.85–2538.80	CO_2, CH_4, O_3, H_2O, HDO				
	2540.10–2540.70	CO_2, CH_4, O_3, H_2O, HDO				
O_3 (3051)	3051.29–3051.90	H_2O, CH_4, HDO, CH_3D	100	20%	2.5/2.1	8.6%/1.5%
O_3 (1000)	1000.00–1000.50	H_2O, CO_2, CH_4, O_3 isotopes	35	20%	4.8/3.2	5.4%/1.1%

[a]Spectral fitting microwindows, fitted interfering species, SNR of measurements, diagonal elements of the a priori covariance matrix ($\mathbf{S}_a$), DOFS for total/stratospheric (12–50 km) columns, and errors (total/random) on the 12–50 km partial columns.

the National Centers for Environmental Prediction Climate Prediction Center meteorological data product (hyperion.gsfc.nasa.gov/Data_services/automailer/index.html) for z = 0–50 km and the mean of a 40 year run (1980–2020) of the Whole Atmosphere Chemistry Climate Model (WACCM, version 6) [*Eyring et al.*, 2007] for Toronto (J. Hannigan, NCAR, personal communication, 2012) for z = 50–120 km.

[10] The TAO O_3, HCl, and N_2O measurements have been validated during a number of ground-based and satellite intercomparison campaigns [*Wiacek et al.*, 2007; *Wunch et al.*, 2007; *Taylor et al.*, 2007, 2008]. We have since updated some retrieval parameters such as the a priori VMR profiles, which now come from the mean of the same 40 year WACCM run mentioned above. The spectral microwindows have been updated to those recommended by the Network for Detection of Atmospheric Composition Change Infrared Working Group (NDACC-IRWG) harmonization initiative (which seeks to have all NDACC-IRWG sites use the same retrieval parameters for consistency, www.acd.ucar.edu/irwg/), except those for O_3. One O_3 microwindow used for this study is 1000–1005 cm^{-1}, which is the IRWG recommendation. But for better temporal coverage for our data set, we also include the 3051.29–3051.90 cm^{-1} O_3 microwindow. Both microwindows provide ample information for stratospheric partial columns, no bias, and have been used in previous studies (e.g., see *Kagawa et al.* [2007] for the 3051 cm^{-1} microwindow and *Lindenmaier et al.* [2010] for the 1000 cm^{-1} microwindow). All microwindows used in this study, except that for HF and the 1000 cm^{-1} microwindow for O_3, fall in the spectral range of the same filter (NDACC FTIR filter 3) and thus are measured at the same time. The microwindow for HF retrievals falls in a different spectral filter (NDACC FTIR filter 1), and the 1000 cm^{-1} microwindow falls in NDACC filter 6. Thus, the HF and some O_3 measurements occur at slightly different times and often have fewer measurements per day than the other species.

[11] Table 1 lists the retrieval parameters used and the resulting median degrees of freedom for signal (DOFS, defined as the trace of the averaging kernel matrix) [*Rodgers*, 2000] for the total columns and the 12–50 km stratospheric partial columns over the 12 year data set. Table 1 also lists the total errors on the 12–50 km partial columns and the random component of the errors (discussed below). The signal-to-noise ratios (SNR) of the measurements (related to the diagonal elements of the error covariance matrix, $\mathbf{S}_e$, with no off-diagonal elements) [*Wiacek et al.*, 2007] were chosen based on a root-mean-square fitting residual versus SNR trade-off curve for each species. The a priori covariance matrices ($\mathbf{S}_a$, diagonal elements of corresponding standard deviation listed in Table 1) for each species were chosen based on the variance seen in the respective Halogen Occultation Experiment observations over Toronto [*Wiacek et al.*, 2007], except for N_2O, which was based on Michelson Interferometer for Passive Atmospheric Sounding observations, and we use a Gaussian correlation length of 4 km for off-diagonal elements of $\mathbf{S}_a$ [*Wiacek*, 2006; *Wiacek et al.*, 2007].

[12] The stratospheric columns (defined as 12–50 km in this study) of HF, HCl, O_3 (at 3051 cm^{-1} and 1000 cm^{-1}), and N_2O have errors of 3%, 3.5%, 8.6%, 5.4%, and 9%, respectively. These are total error budgets that include spectroscopic errors (line width and line intensity, which together are the dominant sources of error), measurement, smoothing, temperature, interference, and solar zenith angle errors calculated as described in *Lindenmaier et al.* [2010]. When only random errors (eliminating spectroscopic errors which are systematic) are taken into account (i.e., when discussing changes within the time series), the errors are 1.1%, 2.0%, 1.5%, 1.1%, and 1.8% for HF, HCl, O_3 (at 3051 cm^{-1} and 1000 cm^{-1}), and N_2O, respectively. These are summarized in Table 1.

[13] Because FTIR solar absorption measurements can only be made when skies are clear, at TAO we typically have 80 to 100 days of measurements per year, with greater coverage in the summertime and a greater number of measurement days in recent years due to improvements in efficiency and instrument maintenance.

[14] Detecting polar vortex intrusions using ground-based FTIR spectroscopy has few advantages over the other measurement techniques described in section 1: it can be used to measure multiple trace gases simultaneously, or nearly so, including HF; it has sensitivity extending to the upper stratosphere; and it can provide data sets that cover long time periods (e.g., semiregular measurements at TAO since 2002).

2.1.1. FTIR Sensitivity to the Stratosphere

[15] The TAO averaging kernels characterize the vertical information contained in the FTIR retrievals [*Rodgers*, 2000]. Figure 1 shows typical TAO VMR averaging kernels for total column HF, HCl, O_3, and N_2O retrievals along

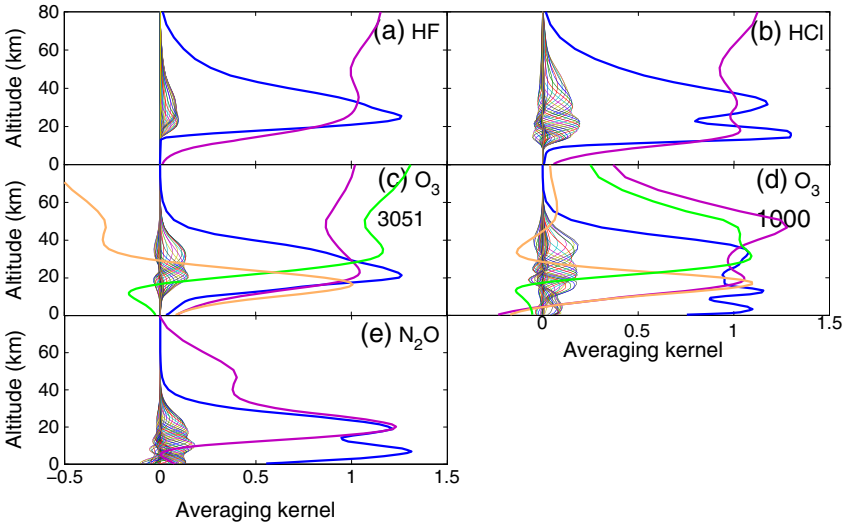

Figure 1. VMR averaging kernels (thin colored lines), sensitivity (thick blue lines), and stratospheric partial column (12–50 km) averaging kernels (thick purple lines) for TAO retrievals of (a) HF, (b) HCl, (c) O_3 (from 3051 cm^{-1} microwindow), (d) O_3 (from 1000 cm^{-1} microwindow), and (e) N_2O. In Figures 1c and 1d, the O_3 partial column averaging kernels for 12–23 km and 23–50 km are shown in orange and green, respectively.

with the stratospheric partial column (12–50 km) averaging kernels, which are equal to the VMR averaging kernels weighted by the density, summed over the layers of interest. The weighting by density, along with some smearing of information to higher altitudes, is what causes the partial column averaging kernel to increase at higher altitudes for HF, HCl, and O_3. Also plotted is the sensitivity, S_k, at each altitude, k (equation (1)) [*Vigouroux et al.*, 2008]:

$$S_k = \sum_i A_{ki}, \tag{1}$$

where A is the averaging kernel matrix and the summation is over the i elements of the kth row. When the sensitivity is above 0.5, it means that the measurements are contributing more than 50% to the retrieved profile (with the rest coming from the a priori profile). The HF, HCl, and O_3 retrievals all have excellent sensitivity ($S_k \sim 1$) in the stratosphere. While the N_2O retrievals have more sensitivity to the troposphere, S_k is > 0.5 throughout most of the stratosphere, and the DOFS is 1.8 for the 12–50 km partial columns (see Table 1). Thus, the N_2O retrievals have good sensitivity in the stratosphere as well.

[16] About 80% of the stratospheric columns (12–50 km) come from 12–35 km (380–1000 K), 12–32 km (380–850 K), 12–20 km (380–500 K), and 12–32 km (380–850 K), for HF, HCl, N_2O, and O_3, respectively.

2.2. CARE FTIR Spectrometer

[17] Environment Canada's Centre for Atmospheric Research Experiments (CARE) is located at Egbert, Ontario, about 80 km north of Toronto at 44.23°N, 79.78°W, 251 masl. Measurements with a Bomem DA8 FTIR spectrometer began at CARE in January 1996, although we only examine the data set from 2002 onwards when we have complementary TAO data. The CARE DA8 has the same characteristics as the DA8 spectrometer at TAO, and HF, HCl, O_3, and N_2O stratospheric columns were retrieved in the same way as described in section 2.1 and using the parameters in Table 1. The errors of the Egbert stratospheric columns are also the same as those for TAO. The Egbert results complement those from TAO, as the two sites are generally close enough to be looking at the same stratospheric air. That is, the two sites are less than 1° apart, which is the resolution of the MIMOSA and MERRA maps. Theoretically though, a small filament could be over one site and not the other.

[18] The frequency of Egbert measurements varies greatly from year to year due to the availability of staff and instrument downtime for maintenance, repair, and upgrades. The greatest number of measurement days (about 30 per year) occurred during 2002–2007, and there were very few in 2008–2010 and none in 2011–2013.

2.3. OSIRIS

[19] We use O_3 partial columns (12–50 km) from the Optical Spectrograph and infrared Imaging System (OSIRIS) on the Odin satellite [*Llewellyn et al.*, 2004; *Murtagh et al.*, 2002] over the Toronto region (within 600 km, or approximately 5°, of Toronto, 43.66°N, 79.40°W) to complement our TAO and CARE O_3 time series. These data are available from November 2001 to the present and have previously compared favorably to TAO O_3 [*Taylor et al.*, 2007]. We also use OSIRIS O_3 maps centered over the North Pole to examine O_3 distributions at the time of the observed polar intrusion events. To produce polar maps at fixed potential temperature levels, data were passed through a Gaussian filter with a 12° full width at half maximum onto a 5° × 5° latitude/longitude grid. For each grid point, the angular distance between the grid point and the OSIRIS measurements was calculated. Weights based on the angular distance between the measurements and the grid point were calculated using the Gaussian function. The weighted mean of

OSIRIS measurements at the given grid point was then calculated. If the sum of weights at a given grid point was < 1, the grid point was left empty. The Gaussian filter and the interpolation grid were tested for various cases to ensure that smoothing and interpolation did not introduce any spurious features in the maps. The 5° filter provided the best balance between showing the details in the OSIRIS measurements and not leading to large gaps in the figure. The choice of interpolation grid did not have a significant impact on the maps for the measurement dates considered.

[20] OSIRIS observes limb radiance profiles of scattered sunlight from 280 to 800 nm at 1 nm spectral resolution, with a 1 km vertical field of view over tangent altitudes ranging from approximately 10 to 100 km. Vertical profiles are obtained every 5° along the sun-synchronous satellite track inclined at 98° and are nominally measured in the orbit plane, limiting the maximum latitude coverage to 82°. Approximately 15 orbits are performed each day, providing measurements every 24° of longitude at the equator and much denser coverage at high latitudes. OSIRIS measures within 600 km of Toronto several times per day and measures O_3, aerosol, and nitrogen dioxide (NO_2) during the Northern Hemisphere spring and summer (starting in mid to late February for Toronto).

[21] The SaskMART (Multiplicative Algebraic Reconstruction Technique) [*Degenstein et al.*, 2009] v5.01 O_3 product was used in this study. O_3 absorption information in both the UV and visible parts of the spectrum is used to retrieve number density profiles from 60 km to the cloud tops (down to a minimum of 10 km in the absence of clouds). The 12–50 km partial columns were derived from these number density profiles. OSIRIS O_3 mixing ratios, calculated from number density and neutral density profiles, are also available. SaskMART v5.0x O_3 has been well validated, with less than 2% bias compared to other satellite measurements [*Degenstein et al.*, 2009; *Adams et al.*, 2013a, 2013b].

3. Models and Meteorological Analyses

[22] GMI, MIMOSA, MERRA, and DMPs derived from MERRA can be used to trace the location and extent of the polar vortex. We use all of these to confirm the passage of polar vortex air over Toronto in this study.

3.1. Potential Vorticity From MIMOSA and MERRA

[23] We use PV maps centered over the North Pole to determine the location and extent of the polar vortex. PV is an excellent polar vortex tracer because the polar vortex is defined by the polar night jet, and as the vortex spins up in the autumn, PV increases and strong PV gradients form along the vortex edge [e.g., *Nash et al.*, 1996]. PV is conserved on potential temperature surfaces and behaves similarly to a chemical tracer in the absence of diabatic and frictional effects [*Hoskins et al.*, 1985].

[24] We have obtained PV maps from the MIMOSA model and the MERRA data reanalysis for this study. We have also extracted the MIMOSA and MERRA PV time series over TAO's coordinates to look for enhancements in potential vorticity that coincide with the enhancements in our stratospheric partial column measurements.

[25] MIMOSA is a high-resolution (1° by 1°) advection model of PV developed at the Service d'Aéronomie (for a full description, see *Hauchecorne et al.* [2002]). MIMOSA is driven by the European Centre for Medium-Range Weather Forecasts wind fields, which are advected along potential temperature surfaces (ether.ipsl.jussieu.fr/ether/pubipsl/mimosa_uk.jsp). PV is given in potential vorticity units (1 pvu = 10^{-6}K m^2 kg^{-1} s^{-1}). MIMOSA was developed to quantify the effect of transport of polar air on lower stratospheric ozone at midlatitudes [*Marchand et al.*, 2003] and has been shown to be capable of predicting filament locations to within 100 km [*Hauchecorne et al.*, 2002], making it well suited for this study.

[26] MERRA is a long-term meteorological data reanalysis using NASA's Global Modeling and Analysis Office Goddard Earth Observing System Version 5.2.0 (GEOS-5) data assimilation system. It was developed at the NASA Goddard Earth Sciences Data and Information Services Center [*Rienecker et al.*, 2011]. The GEOS-5 system is run at a resolution of 0.5° latitude by 0.67° longitude, but PV for MERRA is output on a reduced resolution grid (1° by 1.25°) and on pressure levels over which PV is not conserved. We interpolate MERRA PV onto potential temperature levels and compare PV at four vertical levels (435 K, 475 K, 675 K, and 950 K) to that from MIMOSA. MERRA and MIMOSA maps agree well despite being based on different meteorological analyses, so the two autonomously confirm the location of the polar vortex and its filaments. MERRA output goes as far back as 1979 and has output every 3 h for each day (in section 4 we present MERRA output at 15 UT on each day, which coincides closely with morning measurements at TAO), whereas MIMOSA output is only available beginning in 2005 and only output at 12 UT on each day. Therefore, only the MERRA fields allow us to check for polar intrusion events in our data set between 2002 and 2004.

3.2. N_2O and O_3 From GMI

[27] Since the chemical lifetime of N_2O in the stratosphere is much longer than dynamical time scales, we use modeled N_2O from the GMI 3-D CTM [*Strahan et al.*, 2007] as another polar vortex tracer. Because N_2O is a passive tracer of air motions, it has been used in previous dynamical studies [e.g., *Orsolini et al.*, 1998; *Orsolini and Grant*, 2000; *Manney et al.*, 2000]. GMI O_3 is also used in this study as its chemical lifetime is long in the lower stratosphere in the absence of heterogeneous chemical O_3 depletion. In section 4, we present GMI O_3 maps in order to both track the location of the polar vortex and assess whether polar O_3 is reduced or enhanced at the time of our events.

[28] GMI includes both tropospheric and stratospheric chemistry and is driven by assimilated meteorological fields from MERRA [*Rienecker et al.*, 2011]. Combined stratosphere-troposphere runs [*Duncan et al.*, 2007] were used in this study, and natural and anthropogenic emissions were both considered. The horizontal resolution of the model is 2° × 2.5°, output on 72 pressure levels, with a lid at 0.015 hPa (∼75 km). We present polar maps interpolated onto four potential temperature surfaces (435 K, 475 K, 675 K, and 950 K) that were produced from the output at 12–12:30 UT.

3.3. Derived Meteorological Products

[29] *Schoeberl and Newman* [1995] have shown that the vertical extent of polar vortex filaments varies greatly.

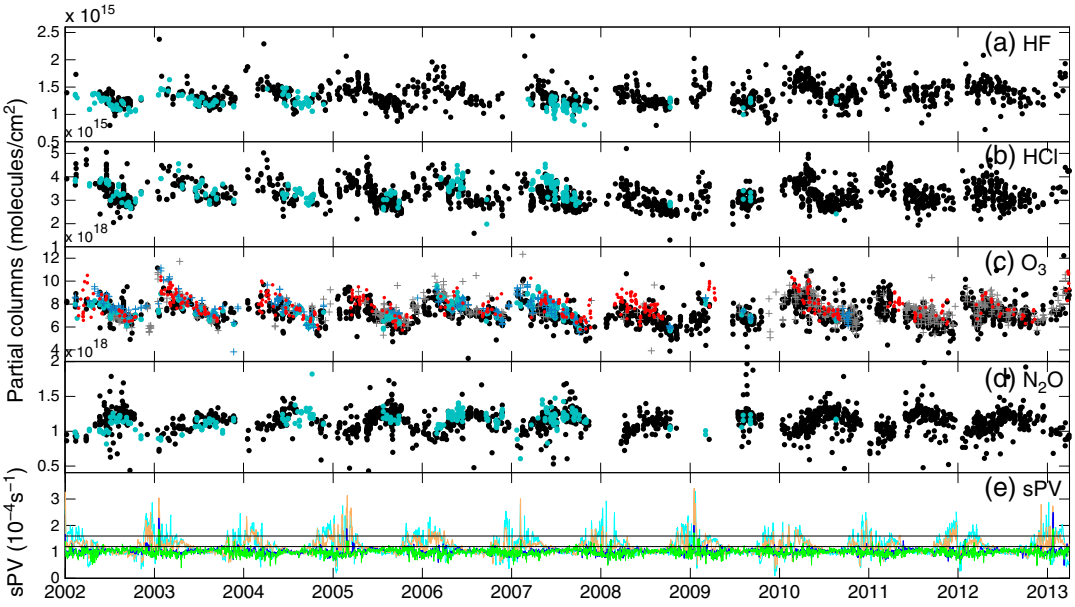

Figure 2. TAO (black), CARE (cyan), and OSIRIS (red) stratospheric partial columns (12–50 km) of (a) HF, (b) HCl, (c) O_3 (from the 3051 cm^{-1} microwindow), and (d) N_2O. In the Figure 2c, the grey and blue crosses are retrievals from the 1000 cm^{-1} microwindow for TAO and CARE, respectively. Figure 2e is scaled potential vorticity over Toronto at 435 K (green), 475 K (blue), 675 K (orange), and 950 K (cyan), and the inner (sPV = $1.6 \times 10^{-4} s^{-1}$) and outer (sPV = $1.2 \times 10^{-4} s^{-1}$) vortex edges are indicated by the upper and lower horizontal lines, respectively.

Typically, filaments are shallow (a few kilometers thick), but sometimes they can extend through much of the depth of the stratosphere. In order to determine the vertical extent of our observed polar vortex intrusions, we use DMPs [*Manney et al.*, 2007] based on MERRA meteorological fields, which include temperature, potential temperature, pressure, equivalent latitude (EqL), PV, scaled PV (given in vorticity units (10^{-4} s^{-1}), tropopause height, horizontal winds, and vortex edge location, all interpolated to the measurement locations. Equivalent latitude is the latitude that would enclose the same area between it and the pole as a given PV contour [*Butchart and Remsberg*, 1986; *Manney et al.*, 2007]. The vortex edge is defined as in *Manney et al.* [2007] by the EqL of the maximum of the wind speed times the PV gradient. Scaled PV (sPV) is PV divided by $\delta\theta/\delta p$, such that sPV is normalized at all vertical levels in the stratosphere [*Dunkerton and Delisi*, 1986; *Manney et al.*, 1994].

[30] We use the time series of MERRA sPV over Toronto at four stratospheric levels (same as above), and we also examine the vertical profiles of sPV over Toronto during the polar intrusion events to determine the vertical extent over which the polar intrusions occurred. sPV is used to determine when Toronto is inside the polar vortex; the outer edge of the vortex is defined to be at an sPV of $1.2 \times 10^{-4} s^{-1}$, and the inner vortex edge is defined to be at an sPV of $1.6 \times 10^{-4} s^{-1}$ [*Manney et al.*, 2007]. Note that except during vortex breakup, the EqL and sPV methods of determining the vortex edge location agree quite well in the lower stratosphere (which comprises the bulk of the O_3 column) but that no automated vortex edge identification works especially well in the springtime [*Manney et al.*, 2007].

4. Results and Discussion

4.1. Identification and Frequency of Polar Intrusion Events

[31] The complete TAO and CARE time series, from January 2002 until March 2013, of individual measurements of stratospheric HF, HCl, O_3, and N_2O partial columns are shown in Figure 2. These gases have seasonal cycles, with HF, HCl, and O_3 stratospheric columns having maxima in the spring and N_2O stratospheric columns anticorrelated, having maxima in the late summer/early fall. There are also many outliers in the time series (Figure 2) that are associated with good spectral fits and realistic retrieved profiles, and so we would like to determine the causes of some of this atmospheric variability. OSIRIS O_3 partial columns (12–50 km) over Toronto (within 600 km) are included to help fill in the gaps in the FTIR time series, and they agree well with the TAO DA8 O_3 measurements, with only a 5% systematic bias (OSIRIS greater than TAO). Therefore, there is a good connection between the ground-based measurements and the OSIRIS maps that appear in section 4.3. Figure 2 also includes the sPV time series at four vertical levels in the stratosphere: 435 K (∼16 km), 475 K (∼18 km), 675 K (∼25 km), and 950 K (∼32 km), and the two horizontal lines indicate the boundary of the outer vortex edge (at sPV = $1.2 \times 10^{-4} s^{-1}$), and the inner vortex edge (at sPV= $1.6 \times 10^{-4} s^{-1}$). Note that there are more polar intrusions over Toronto in the upper stratosphere (650 K and 950 K) because the polar vortex is typically larger, and filaments tend to tilt away from the pole at higher altitudes [*Schoeberl and Newman*, 1995].

[32] To identify polar intrusion events, we started with the sPV definition of inner and outer vortex edge, and the

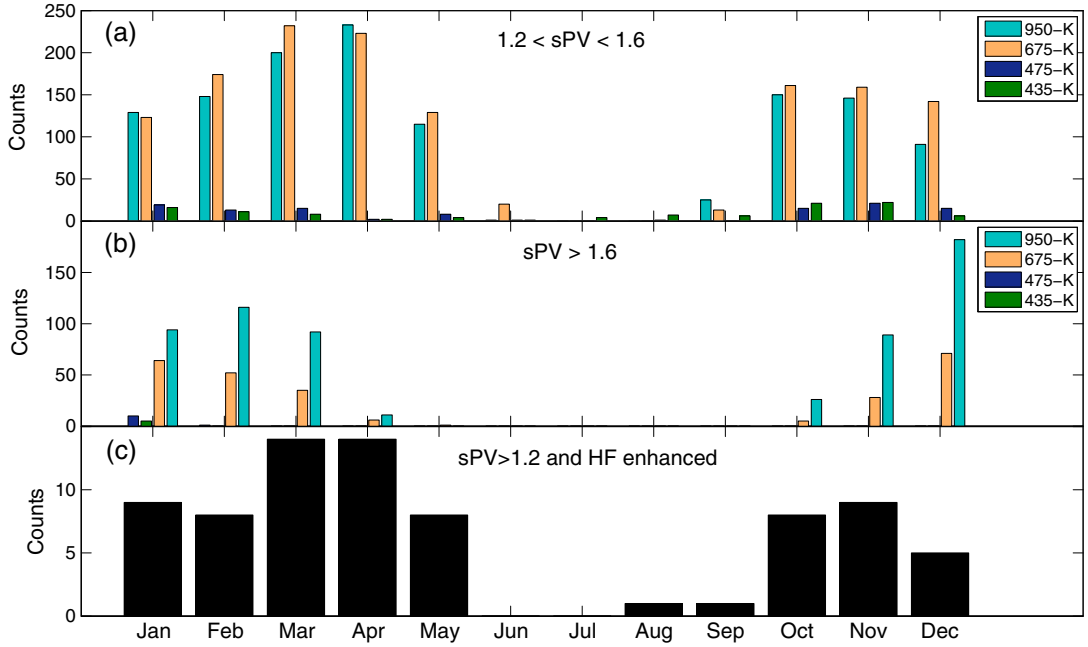

Figure 3. Number of polar intrusion days at four vertical levels (950 K, 675 K, 475 K, and 435 K) over Toronto from January 2002 to March 2013, from the MERRA DMPs, separated by month. sPV is given in 10^{-4} s^{-1}. (a) The number of intrusions that are within the vortex edge region, (b) the number of intrusions that are within the vortex, and (c) the number of intrusion days that met the four criteria described in section 4.1.

sPV time series over Toronto from the DMPs. Scaled PV on the four levels suggests that between January 2002 and March 2013, there were 675 days (16% of days) when the polar vortex (sPV > $1.6 \times 10^{-4} s^{-1}$) passed over Toronto and 1492 days (36% of days) when the edge of the polar vortex ($1.2 \times 10^{-4} s^{-1}$ < sPV < $1.6 \times 10^{-4} s^{-1}$) was over Toronto. Figures 3a and 3b show these days distributed by month, and Figures 4a and 4b show these days distributed by year. Since the FTIR spectrometer cannot measure on cloudy days and has sporadic downtime for maintenance and repairs, the gaps in our data set make it certain that we are not detecting all of these polar intrusion events over southern Ontario. In fact, there are FTIR measurements at TAO on only ~14% of those "enhanced sPV" (> $1.2 \times 10^{-4} s^{-1}$) days. However, while the FTIR data set is missing 86% of the polar intrusions (in enhanced sPV), our subset of measurement days

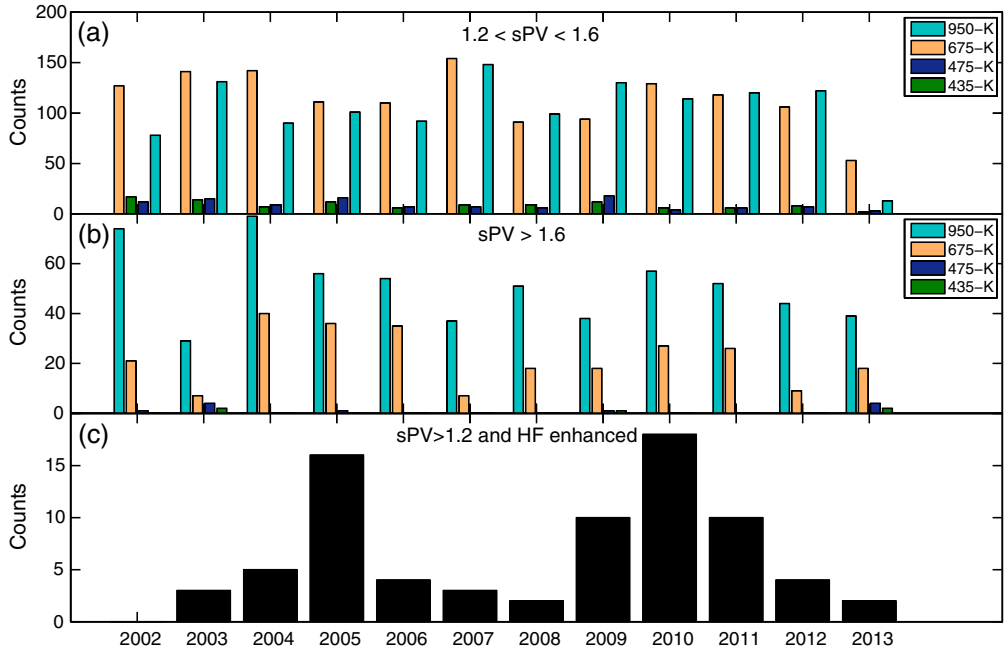

Figure 4. Same as Figure 3 but separated by year.

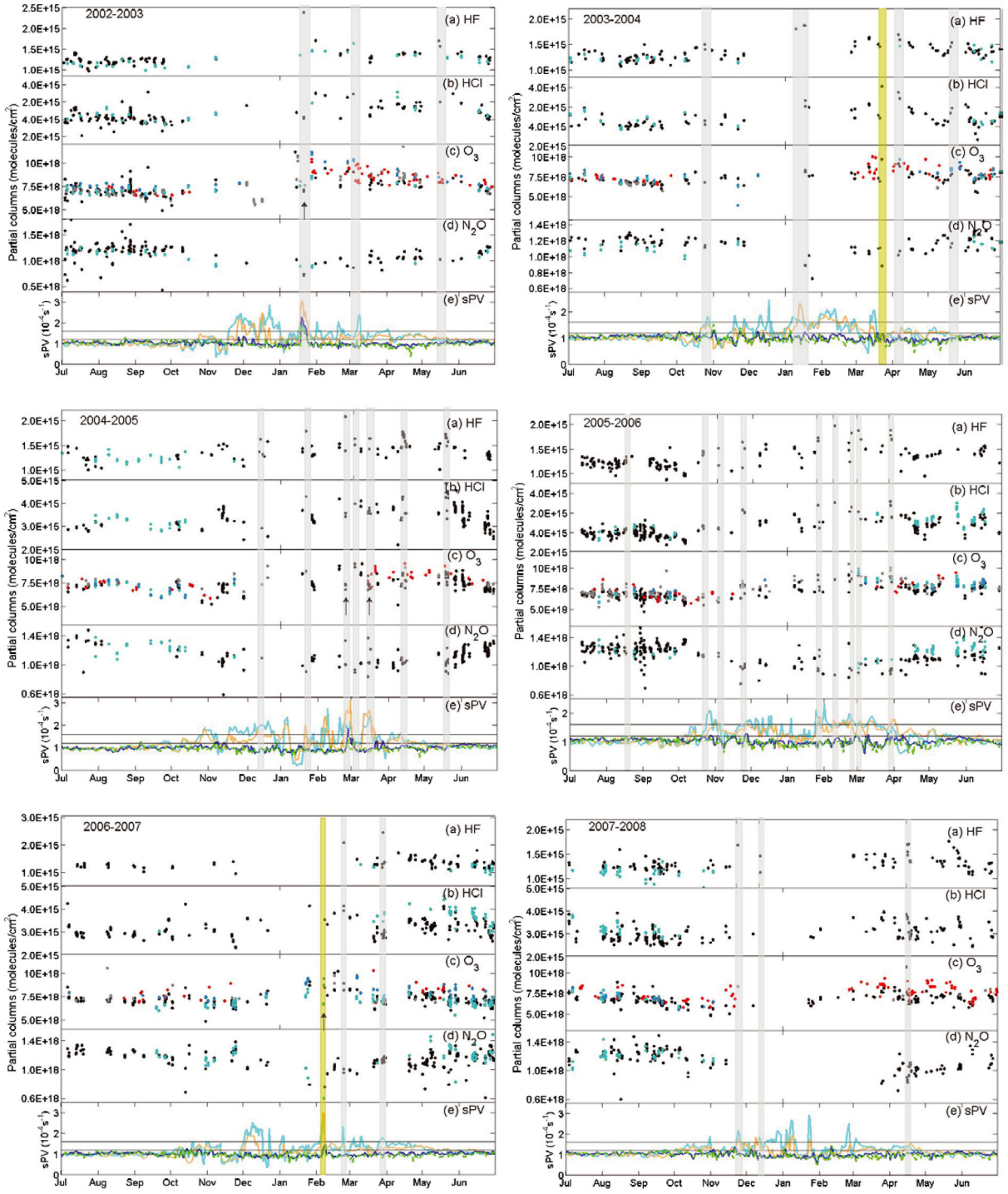

Figure 5. Same as Figure 2 but an expanded view of each year, and 3051 and 1000 O_3 products are combined into black (TAO) and cyan (CARE) points. The total errors on these partial columns are 3% for HF, 3.5% for HCl, 7.5% for 12–23 km O_3, 11.6% for 23–50 km O_3, and 9% for N_2O. Grey and yellow boxes highlight the polar intrusion events (grey showing events that met the four criteria and yellow showing events that met only three of the four criteria).

gets a similar percentage with polar intrusions to that found with the sPV time series.

[33] Since HF is a good dynamical tracer, we expect polar vortex intrusions to cause variability in the FTIR time series (though to a lesser extent if the polar intrusion is shallow and/or much higher than 35 km where it is not contributing a large amount to the column). Therefore, we looked at (1) the HF stratospheric columns that were *enhanced*, defined as when the HF stratospheric column was more than 1σ greater than the monthly mean (in either the singular monthly mean or the climatological (2002–2013) monthly mean). We flagged those days as "enhanced HF" days. Then we

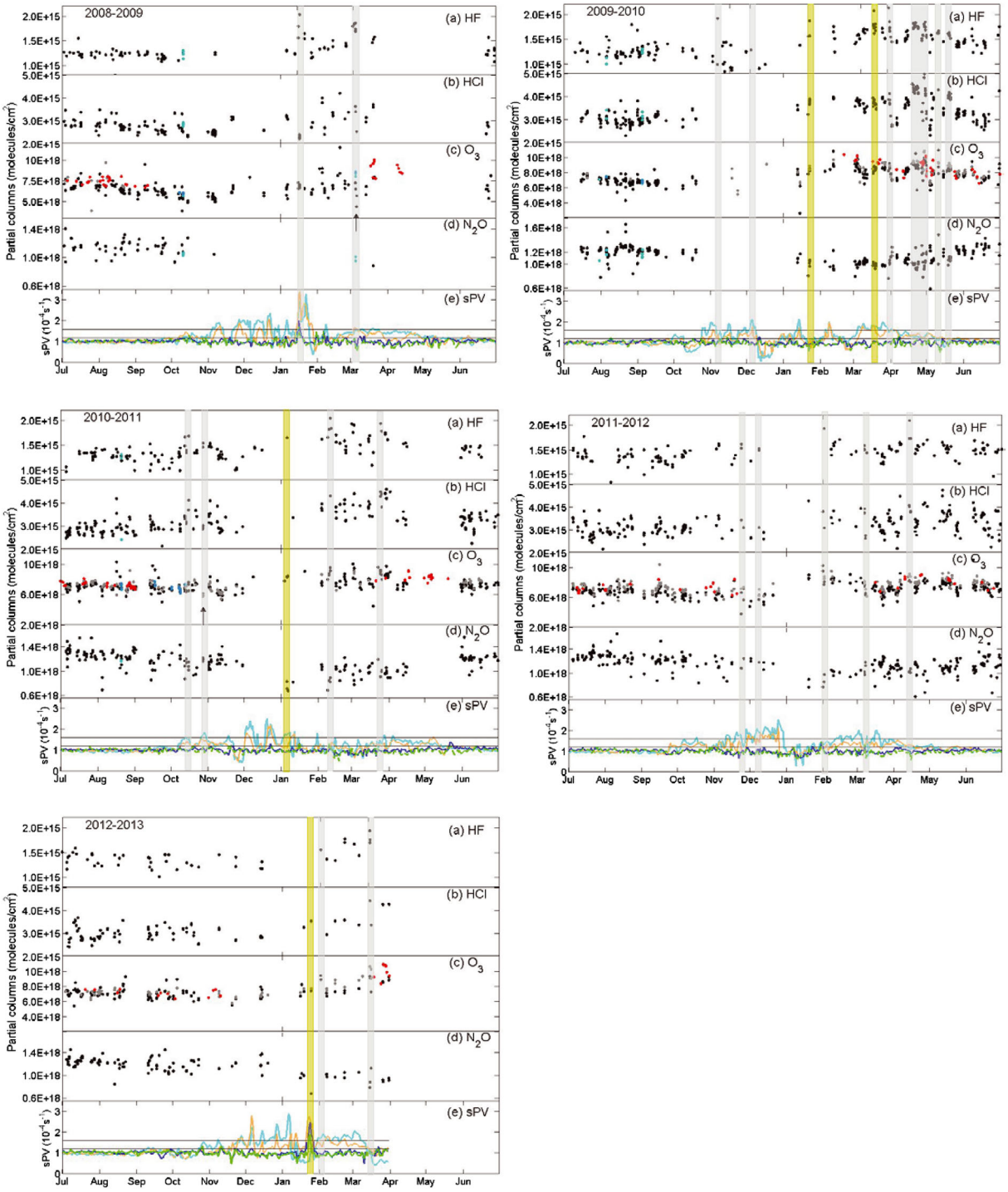

Figure 6. Same as Figure 6 but later years.

determined whether these flagged days also had (2) reduced N_2O stratospheric columns (compared to a few days before and after the event), and (3) sPV > $1.2 \times 10^{-4}s^{-1}$. Finally, (4) we checked the MIMOSA and MERRA PV maps at the four vertical levels in the stratosphere mentioned above to see if there was a vortex excursion or filament over Toronto on those dates. Using these four criteria, we found 47 polar vortex intrusions. Six additional polar intrusions were found that did not quite satisfy all of the criteria. Either there were not enough HF measurements to make the 1σ statistic meaningful (but the HF column was increased, and sPV was $> 1.2 \times 10^{-4}s^{-1}$) or the sPV value was just below $1.2 \times 10^{-4}s^{-1}$ (but the HF column was enhanced and the polar map confirms a filament). Nevertheless, we include those six in our study for a total of 53 "polar intrusion events," on which we focus the rest of our discussion. There were an average of four events detected in the FTIR time series per year. Between November and April inclusive ("winter/spring"), the polar intrusion events consist of 16% of our measurements.

Table 2. Percent Increase in 2003–2012 Stratospheric Column Variability and sPV Variability Over Toronto Due To Polar Intrusion Events[a]

Species	Mean Increase in Variability (2003–2012)
HF (12–50 km)	15.1%
HCl (12–50 km)	7.1%
N_2O (12–50 km)	1.7%
O_3 (12–50 km)	5.7%
O_3 (12–23 km)	3.8%
O_3 (23–50 km)	–0.5%
sPV 435 K	4.4%
sPV 475 K	11.2%
sPV 675 K	14.5%
sPV 950 K	5.2%
sPV 435 K	9.3%
sPV 475 K	14.4%
sPV 675 K	58.8%
sPV 950 K	62.0%

[a]O_3 products are from the 1000 and 3051 microwindows combined. The first set of sPV variability is due to 53 polar intrusion events on sPV during the FTIR measurement days. The second set of sPV variability is due to all polar intrusion days in the sPV time series not constrained by HF measurement days.

[34] The monthly and yearly distribution of these 53 polar intrusion events are shown in Figures 3c and 4(c), respectively. Note that the monthly distribution is similar to the enhanced sPV distribution, with the differences being due to the measurement sampling bias. It turned out that all of the HF enhancements in December through March were during polar vortex intrusions. The HF enhancements in April, May, October, and November were rarely coinciding with a polar vortex intrusion, and only one enhancement in the summer (August 2005) was during a polar intrusion event. This suggests that the December to March variability in the HF time series is due to polar vortex air passing over Toronto. The late spring, summer, and fall variability in HF must be due to other causes, and this variability (in May through September) is about half that during the winter (see section 4.2 for more discussion on HF variability).

[35] Note that no one criterion for *HF enhancements* (e.g., 1σ, median absolute deviation, and absolute cutoff) captured all of the polar intrusion events so there could be more intrusions in the FTIR data set that were missed. Also the DMPs (and hence sPV) are interpolated values; therefore, a slight mismatch in the location of the filament between MERRA and the "truth" could make the difference between considering something inside or outside the vortex [*Fairlie et al.*, 1997; *Manney et al.*, 1998]—hence the six additional days.

4.2. Effect on Trace Gases: Variability

[36] All of the polar intrusion events we found in the measurements are highlighted by the grey (met all four criteria) and yellow (met three out of four criteria) boxes in Figures 5 and 6. These figures show the time series expanded for each year.

[37] The variability introduced in the FTIR time series by the polar intrusion events (Var) for each trace gas in the complete time series is calculated for each year and for the complete time series, with the latter given in Table 2. This table shows the percent differences between the standard deviations calculated from our FTIR measurements with (σ_{with}) and without (σ_{wout}), the polar intrusion events:

$$\mathrm{Var} = \frac{\sigma_{with} - \sigma_{wout}}{\sigma_{with}} \times 100\%. \quad (2)$$

The upper stratospheric O_3 value in Table 2 is negative; this means that the polar intrusion events *decreased* the variability in the time series. The magnitude of the negative value is small (< –0.5%), which may just be interpreted as a negligible effect on the time series variability. However, O_3 variability can be reduced by the following scenarios: (i) the polar vortex filament may have a similar amount of O_3 to that in unperturbed midlatitude air or (ii) a springtime polar vortex filament may have O_3-poor air, making the column more like the summertime O_3 columns (when there is a seasonal minimum and more FTIR measurements).

[38] From 2003 to 2012, polar intrusion events cause a mean increase in variability of 15.1%, 7.1%, and 5.7% for stratospheric HF, HCl, and O_3, respectively. We left out 2002 and 2013 from our calculations because early 2002 was before regular daily measurements commenced at TAO, and therefore, there were very few measurements during January to April 2002, and the 2013 data set is not yet complete.

[39] The variability introduced by the polar vortex intrusions is greatest for HF, consistent with it being a good dynamical tracer. For example, in January 2003, we have one of the highest outliers in the HF (and N_2O) columns (Figure 5), which occurred when the polar vortex was over Toronto for the largest altitude range (see mauve line in Figure 12). In this year, the polar intrusions caused a 35% increase in HF variability. The variability of HCl is less sensitive to the polar vortex intrusions in most years, likely because dynamical enhancements of HCl can be offset by chemical processing. However, HCl is still significantly affected by polar vortex air, consistent with *Coffey et al.* [2008]. The polar vortex intrusions have a smaller effect on the variability of O_3 because the amount of O_3 in the filaments is not consistently greater than (like HF and HCl) or less than (like N_2O) that in midlatitude air. The amount of O_3 in a filament is influenced by the altitude range at which it occurs, the dynamics of the polar vortex system, and chemical processing. Finally, the small effect on N_2O variability is likely due to the smaller altitude range that contributes to the N_2O stratospheric column (see end of section 2.1.1). Therefore, only lower stratospheric polar intrusions would have a significant effect on the N_2O time series.

[40] Figure 7 shows the variability (given by the standard deviation from the climatological monthly mean) of each species for the complete time series (black circles) and the time series without the polar intrusion events (red crosses). In addition to Table 2, this figure shows that the largest effect on variability occurs for HF, during the winter and early spring months. Figure 7 illustrates that there is about twice as much variability in the HF time series in the winter as there is in the summer and that about half of the increase of the winter variability compared to summer is due to the polar intrusion events.

[41] The variability in sPV at four different levels (435 K, 475 K, 675 K, and 950 K) was also calculated and included in Table 2 and Figure 7. The first set of sPV values in Table 2 are results when we only consider the 53 events and their effect on sPV during the FTIR measurement days. The

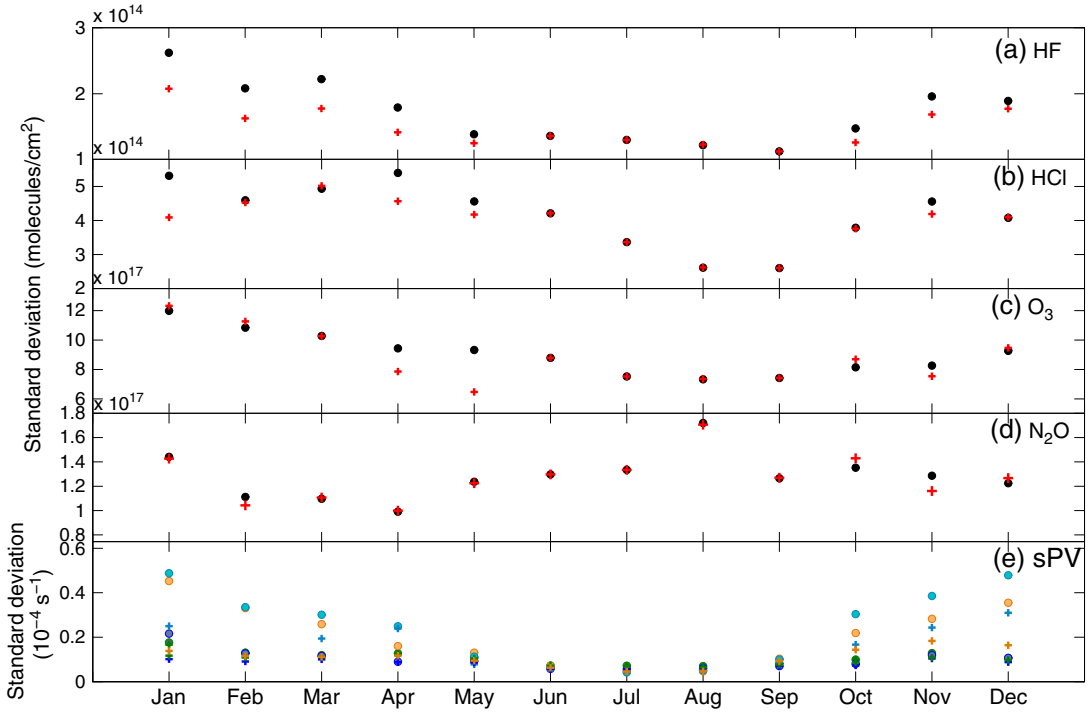

Figure 7. Variance in TAO stratospheric partial columns of (a) HF, (b) HCl, (c) O_3, (d) N_2O, and in (e) sPV, as given by the standard deviation from the climatological monthly mean for each month. Circles are for the full time series, and crosses are for the time series without the polar intrusion events. In Figure 7e, 435 K is green, 475 K is blue, 675 K is orange, and 950 K is cyan, and the crosses are for the time series without the enhanced sPV days.

second set of sPV values are the results if we are not constrained to FTIR measurement days and consider the full sPV time series during which there are a total of 2167 polar intrusion days from January 2002 to March 2013. When all of these are taken into account, their effect on sPV variability is 9.3%, 14.4%, 58.8%, and 62.0% at 435 K, 475 K, 675 K, and 950 K, respectively, and Figure 7 shows this effect by month (with circles showing the variability on the full sPV time series and crosses showing the variability on the sPV time series without the enhanced sPV days). Note that the monthly HF variability with and without polar intrusion events follows a very similar shape to the sPV variability (Figures 7a and 7e), which supports the use of FTIR HF columns to detect polar vortex intrusions.

4.2.1. Effect on O_3 Columns

[42] Generally speaking, stratospheric O_3 columns above Toronto are slightly greater during the polar intrusion events, consistently agreeing with the GMI model, the Microwave Limb Sounder (MLS) on the Earth Observing System Aura satellite, the Earth Probe/Total Ozone Mapping Spectrometer (EP/TOMS), the Ozone Monitoring Instrument (OMI), and OSIRIS O_3 measurements. The O_3 stratospheric columns can be split into 12–23 km and 23–50 km, as these partial columns have at least 1 DOFS each. Though not shown in Figures 5 and 6, these lower and upper stratospheric partial columns provide more insight into which region of the stratosphere any changes to the O_3 column are occurring. The total errors on these partial columns are 7.5% (12–23 km) and 11.6% (23–50 km) for the 3051 microwindow and 9.0% (12–23 km) and 5.7% (23–50 km) for the 1000 microwindow. When only random errors are considered, they are 2.6% (12–23 km) and 2.3% (23–50 km) for the 3051 microwindow and 2.0% (12–23 km) and 2.1% (23–50 km) for the 1000 microwindow.

[43] In 2005, 2010, and the total time series, there were significant (greater than the standard error in the O_3 partial columns) changes in the average of our stratospheric O_3 columns due to the polar intrusion events. The only significant *decreases* in annual stratospheric O_3 columns due to the polar intrusion events were in the 23–50 km partial

Table 3. Percent Change in Stratospheric Columns of O_3 Over Toronto Due To Polar Intrusion Events for the Given Year and for the Total Time Series (2002 to 2013)[a]

Partial Column	2003	2004	2005	2006	2007	2008	2009	2010	2011	2012	Total (2003-2012) mean
12-50 km	–1.3%	2.3%	2.1%	4.2%	0.3%	1.4%	0.3%	**15.3%**	–3.3%	5.1%	**4.5%**
12-23 km	1.0%	2.9%	**7.3%**	5.7%	0.0%	1.5%	5.8%	**14.9%**	–1.2%	3.3%	**4.8%**
23-50 km	**–4.2%**	–0.5%	**–7.0%**	–1.4%	0.4%	–0.1%	**–6.5%**	–2.9%	–2.1%	1.3%	–0.9%

[a]Bold values highlight changes that are greater than the standard error of the mean difference.

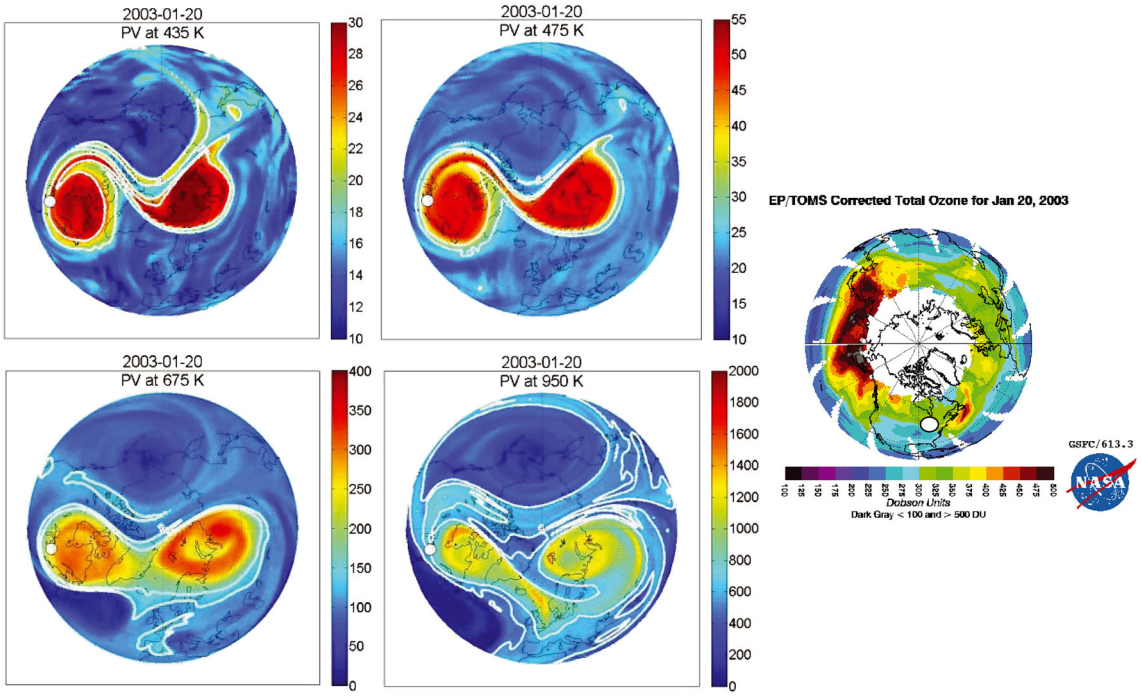

Figure 8. Polar intrusion event on 20 January 2003. MERRA PV (in pvu) at 435 K, 475 K, 675 K, and 950 K. The EP TOMS total O_3 column map is also shown (note that this map is oriented 90° counterclockwise compared to the MERRA maps). White circles on each map represents the location of Toronto/Egbert. White contours denote the inner and outer vortex edge limits.

columns in 2003, 2005, and 2009. These changes in O_3 are summarized in Table 3 and were calculated using

$$\text{Change} = \frac{\overline{O_{3\text{with}}} - \overline{O_{3\text{wout}}}}{\overline{O_{3\text{with}}}} \times 100\%, \quad (3)$$

where $\overline{O_{3\text{with}}}$ and $\overline{O_{3\text{wout}}}$ are the means of the stratospheric O_3 partial columns for a given year, with and without the polar intrusion events, respectively. The bold values in Table 3 indicate that the changes in O_3 are greater than the standard error on $\overline{O_{3\text{with}}}$. However, since our FTIR measurements are neither frequent nor uniform in time, these statistics apply only to our data set and should not be interpreted as representing the increase/decrease in O_3 over the Toronto region that would be observed in a continuous data set.

4.3. Effect on Trace Gases: Case Studies

[44] As mentioned in section 4.1, polar PV maps from MERRA and MIMOSA (when available) were used to verify structures extending from the polar vortex southward over the Toronto region. Figures 8 to 11 present these maps for four sample polar intrusion events at the vertical levels at which the intrusion occurred. In these maps, Toronto's location is marked by a white circle, and two white contours indicate the inner and outer vortex edges (equivalent to the horizontal black lines in Figures 2, 5, and 6). In Figures 9 to 11, the shape of the polar vortex and its filaments given by MERRA PV were confirmed with the MIMOSA PV maps (for which the magnitudes of PV are also similar) and modeled N_2O from GMI. Also from GMI is modeled O_3, which will be discussed below.

[45] For all 53 polar intrusion events, the VMR of N_2O given by GMI is much lower inside the polar vortex and filaments compared to midlatitudes as discussed in section 1 (see Figures 9 to 10 for four examples). Recall that GMI is driven by MERRA meteorological fields; therefore, we would expect the GMI maps to agree well with MERRA PV maps, which is why we also include MIMOSA PV in this study as a more independent check on the location of the polar vortex and its filaments.

[46] Section 4.3.1 discusses the impact of polar intrusions on Toronto area O_3 using three case studies. The first two (January 2003 and February 2007) are examples of when polar O_3 depletion caused a reduction in stratospheric O_3 over Toronto, and the third (March 2011) is an example of when polar O_3 depletion did not have an effect on Toronto stratospheric O_3. Section 4.3.2 discusses an example of stratospheric warming causing the polar vortex to split apart.

4.3.1. Impact on O_3

[47] Unlike some previous studies that focus on reduced O_3 at midlatitudes [*Marchand et al.*, 2003; *Millard et al.*, 2003; *Konopka et al.*, 2003; *Keckhut et al.*, 2007], we find that the majority of the polar intrusion events identified over Toronto resulted in either a small increase or a negligible change in the O_3 stratospheric columns (consistent with *Newman et al.* [1996], *Orsolini et al.* [2001], *Godin et al.* [2002], and *Hauchecorne et al.* [2002]). *Marchand et al.* [2003] modeled the effect of chemically depleted polar vortex air on northern midlatitudes with MIMOSA-CHIM (MIMOSA with chemistry) and reported that midlatitude O_3 VMRs became increasingly affected by the polar vortex starting from around March (when it was responsible for 15% of diminished O_3 at 475 K from 45°–55°N), reaching a maximum in April (when it was responsible for 50% of the diminished O_3 at 475 K from 45°–55°N). Since the

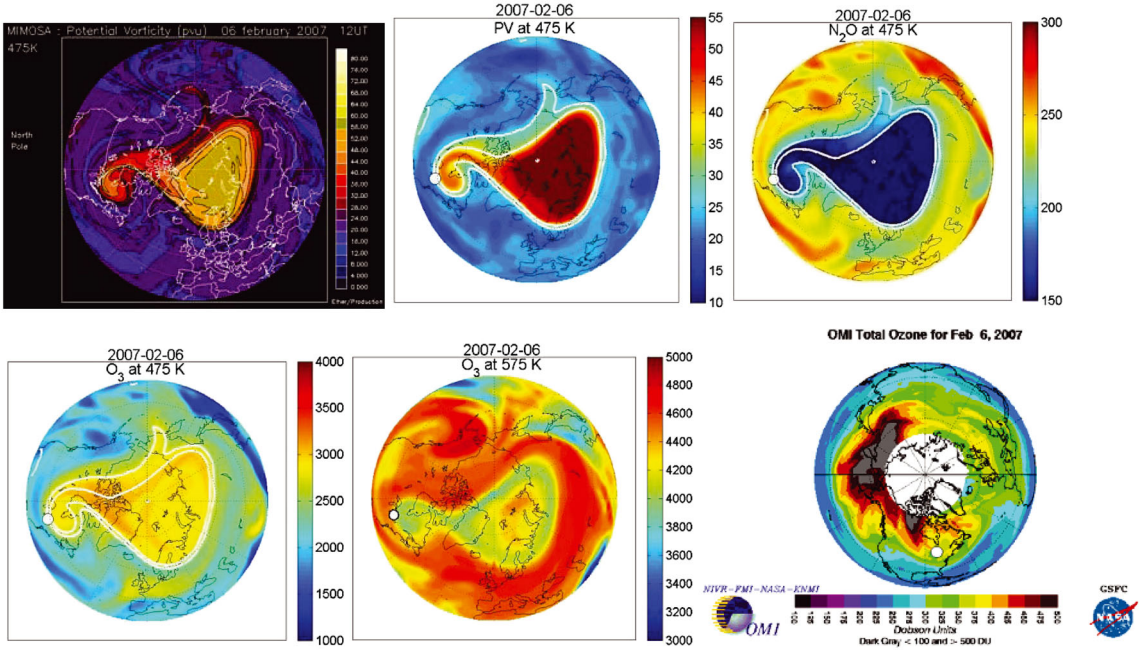

Figure 9. Polar intrusion event on 6 February 2007. (top) MIMOSA PV, MERRA PV (both in pvu), and GMI N_2O (in ppbv). (bottom) GMI O_3 at 475 K and 575 K (both in ppbv) and OMI total column O_3 (note that the OMI map is oriented 90° counterclockwise compared to the other maps). White circles denote the location of Toronto/Egbert. White contours denote the inner and outer vortex edge limits.

Toronto region is located just south of their reported latitude band and most of our polar intrusion events occurred in March or before, we would expect polar intrusions to have less of an effect on our O_3 columns. *Marchand et al.* [2003] also reported negligible O_3 reductions in the filament structures (rather than vortex excursions). Since most of our events were filaments, our findings are consistent with the *Marchand et al.* [2003] study, as reduced O_3 columns were rarely measured as a result of a filament over Toronto.

[48] We only found reduced O_3 columns during six of the 53 polar intrusion events: on 20 January 2003, 23 February 2005, 15–16 March 2005 (both 2005 events supported by *Rösevall et al.* [2008]), 6 February 2007, 3–4 March 2009, and 27 October 2010 (see arrows in Figures 5 and 6). The lower (12–23 km) and upper (23–50 km) stratospheric columns were affected differently during these six events, with about half having a drop in the lower stratospheric partial column and little change in the upper stratospheric partial column, and the other half having a drop in the upper stratospheric partial column and little change in the lower stratospheric partial column. Two of these events are discussed in more detail below.

[49] On 20 January 2003, we have FTIR observations of reduced O_3 in the 12–50 km (Figure 5) and 23–50 km partial column, and MERRA PV maps showing a large filament over Toronto at all four levels (Figure 8) due to a vortex split during a major stratospheric warming [*Jayanarayanan et al.*, 2011], but there are no O_3 observations by OSIRIS on this date nor is there GMI output. O_3 total column observations from EP/TOMS exist (from ozoneaq.gsfc.nasa.gov) and are shown in Figure 8 (note the different orientation of the map). In this figure there is a large amount of O_3 to the west of the polar vortex structure (over western Canada and over the Pacific ocean) which represents regular midlatitude O_3, but where the intrusion occurs (over Ontario and Quebec), the O_3 total columns are reduced, in agreement with our ground-based measurements. The winter of 2002/2003 had appropriate conditions for chemical O_3 loss inside the vortex through late January, as it was cold [*WMO*, 2007], and Arctic O_3 depletion was reported [e.g., *Christensen et al.*, 2005; *Singleton et al.*, 2005; *Jayanarayanan et al.*, 2011]. The HCl stratospheric column is also decreased (Figure 5), which is consistent with chemical ozone loss, as it implies that Cl is activated.

[50] On 6 February 2007 the CARE O_3 12–50 km partial column is reduced (Figure 5). The MIMOSA and MERRA PV maps and the GMI N_2O and O_3 maps at 475 K (Figure 9) all show a large filament over our region, but the GMI 475 K map on 6 February 2007 has *enhanced* O_3 compared to the surrounding midlatitudes. However, the GMI 575 K (~23 km) O_3 map does show reduced O_3 in both the vortex and filament. There is no OSIRIS coverage over the Northern Hemisphere during early February to compare with GMI, but *Rösevall et al.* [2007], *Sonkaew et al.* [2011], and *Søvde et al.* [2011] report significant Arctic O_3 depletion that winter, including on the date of our observation at the 575 K level. Observations of O_3 from MLS at 490 K (not shown) show vortex O_3 that is comparable to midlatitude O_3 (http://mls.jpl.nasa.gov/plots/mls/mls_plot_locator.php) consistent with the GMI 475 K map. The O_3 total column map from OMI (from ozoneaq.gsfc.nasa.gov) is shown in Figure 9 and supports our ground-based measurements, as the O_3 columns in the polar vortex region (including the filament over Ontario and Quebec) are smaller than the O_3 columns at other midlatitudes (e.g., over the rest of Canada).

[51] In contrast to the events on 20 January 2003 and 6 February 2007 discussed above, polar intrusions on 23

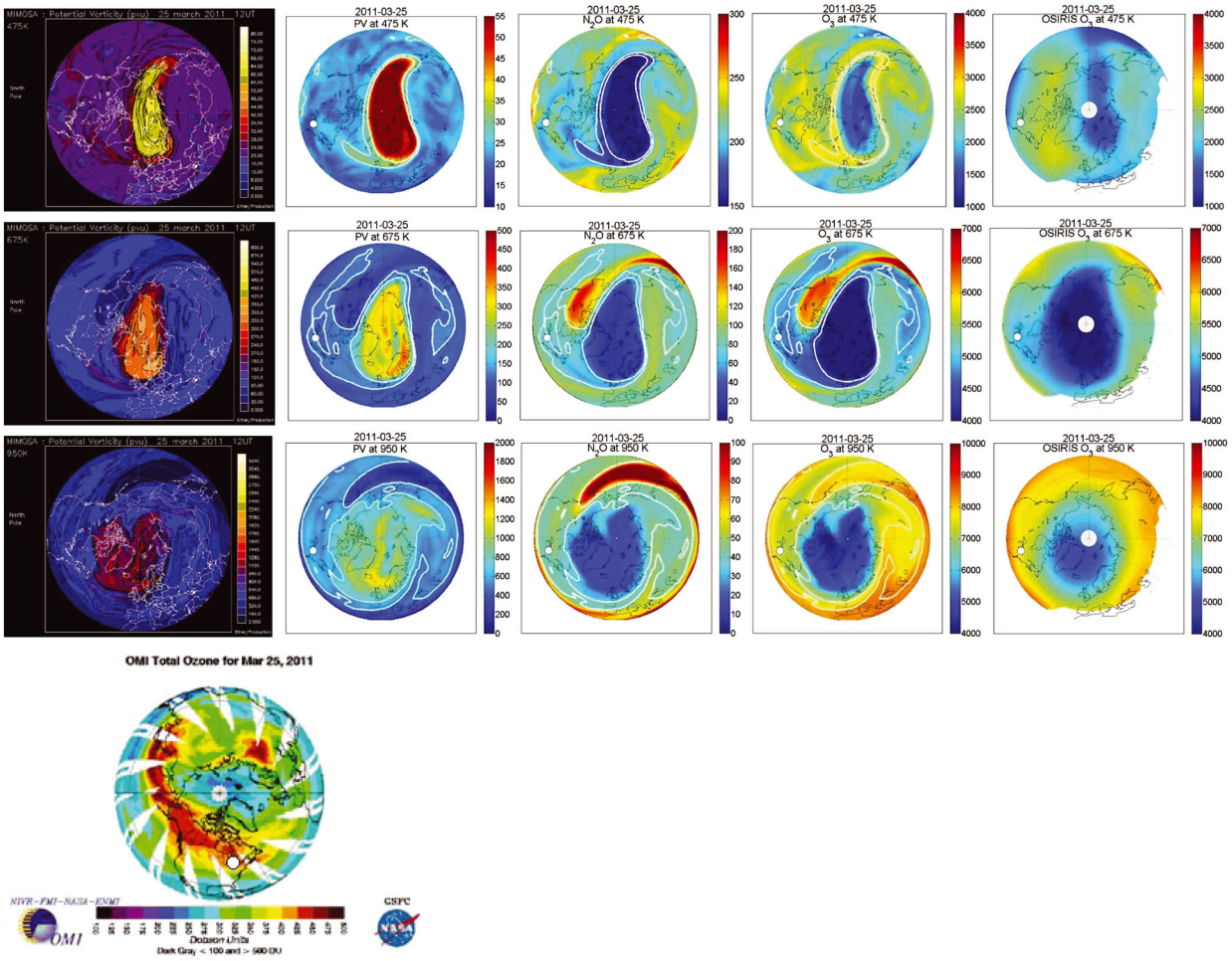

Figure 10. Polar intrusion event on 25 March 2011. (from left to right) MIMOSA and MERRA PV (both in pvu), GMI N_2O and O_3 (both in ppbv), and OSIRIS O_3 (also in ppbv). (bottom) OMI O_3 total column (note the different orientation). (from top to bottom) 475 K, 675 K, and 950 K. White circles denote the location of Toronto/Egbert. White contours denote the inner and outer vortex edge limits.

February 2007 and 23–25 March 2011 do not show reduced O_3 columns (Figures 5 and 6), which might have been expected given the chemical O_3 depletion observed in the polar vortex by *Rösevall et al.* [2007] in 2007 and *Manney et al.* [2011] in 2011. In these cases, O_3 was not reduced in the vortex filaments, which extended over Toronto (e.g., the 25 March 2011 case shown in Figure 10, first and last rows). It would seem that the filaments were not O_3 poor because O_3 depletion was not uniform throughout the vortex. For example, at the end of March 2011, the vortex was O_3 poor near the center but not around its edge (see O_3 in top row of Figure 10). The filament originated from the edge region; therefore, the filament has enhanced O_3 compared to midlatitude air. In contrast, on 6 February 2007 (discussed above), the O_3-poor air is located near the edge of the polar vortex at 575 K; hence, its filament is also O_3 poor (Figure 9).

[52] The polar intrusion event on 23–25 March 2011 is shown for one day in Figure 10 at 675 K and 950 K, which are the levels where the polar intrusion occurred, and 475 K, which is approximately where the peak contribution to the O_3 stratospheric column occurs. The OSIRIS O_3 maps are also shown for this day, confirming the GMI results, and the OMI total column O_3 is shown, confirming reduced O_3 inside the polar vortex, but not in the filament that passed over Toronto.

4.3.2. Impact of a Stratospheric Warming

[53] Similar to January 2003 (Figure 8), January and February of 2009 had interesting polar vortex activity, when a major mid-winter warming occurred [*Manney et al.*, 2009; *Labitzke and Kunze*, 2009], and the vortex split in two, one half passing over southern Ontario in early February. The maps in Figure 11 show the beginning of this breakup, and the polar vortex is already over Toronto as early as 16 January 2009. Figure 6 shows the effect on the FTIR columns. The HCl stratospheric column is decreased. The upper stratospheric O_3 columns (23–50 km) were reduced, while the lower stratospheric O_3 columns (12–23 km) were enhanced (not shown), resulting in the stratospheric O_3 columns (12–50 km) being unchanged (shown in Figure 6). These results are consistent with the GMI modeled O_3, though the OMI total column O_3 appears to be slightly reduced in the polar vortex region (Figure 11).

4.4. Vertical Structure of Polar Intrusion Events

[54] Figure 12 shows the vertical extent of the 53 polar intrusion events in sPV. The vertical grey lines in Figure 12

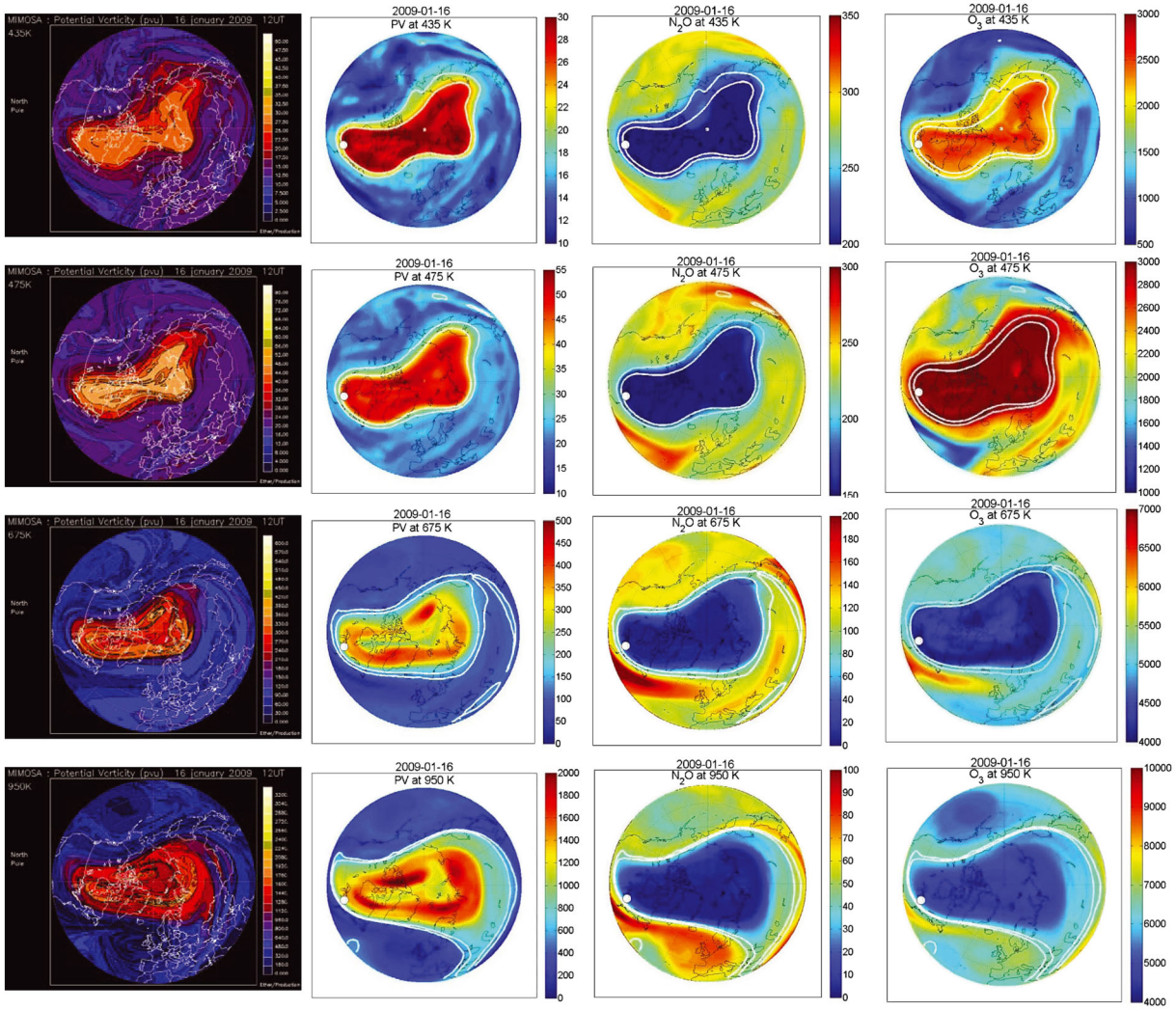

Figure 11. Polar intrusion event on 16 January 2009. (from left to right) MIMOSA and MERRA PV (both in pvu), GMI N_2O and O_3 (both in ppbv), and the OMI total O_3 column map is also shown (note the different orientation). (from top to bottom) the intrusion is shown at 435 K, 475 K, 675 K, and 950 K. White circles denote the location of Toronto/Egbert. White contours denote the inner and outer vortex edge limits.

indicate the outer and inner polar vortex edges, as given by the sPV criterion described in section 3.3. The mean sPV profile from nonintrusion ($sPV < 1.2 \times 10^{-4} s^{-1}$) days and its standard deviation are the thick black lines shown for comparison. Most of the polar intrusion events have sPV values that are within the edge region, but at least half of our 53 events have even higher sPV values, putting them well inside the polar vortex at some part of the profile. In most cases, sPV tends to be large compared to the nonevent mean from about 370 to 1500 K (or 12 to 45 km), which coincides with the vertical range over which the FTIR retrievals are sensitive (see Figure 1 and section 2.1.1).

[55] These results indicate that FTIR partial column measurements provide useful information for polar intrusion detection. Previous publications describing midlatitude polar intrusion events have presented trace gas vertical profiles from aircraft, lidar, and balloon-borne in situ measurements [*Newman et al.*, 1996; *Orsolini et al.*, 2001; *Godin et al.*, 2002; *Durry and Hauchecorne*, 2005; *Tripathi et al.*, 2006]. However, these aircraft, lidar, and balloon measurements were limited to the lower stratosphere (about 10–30 km or 350–800 K), which may miss events that occur between 30 and 50 km (~800–2200 K) (e.g., the 14 May 2003 and 14 December 2004 events detected in this study—red and dark green lines in Figure 12, respectively). For HF, HCl, N_2O, and O_3, the 30–50 km partial columns contain about 45%, 27%, 2%, and 30% of the stratospheric (12–50 km) columns, respectively.

[56] The vertical thickness of the intrusions ranges from about 5 km (e.g., 3 March 2005—orange line in Figure 12) to about 30 km (e.g., 16 January 2009—pink line in Figure 12), and there is often more than one peak in the vertical profiles of sPV (e.g., 27 October 2010—light green line in Figure 12), indicating vortex filament structures occurring at more than one level. These results for vertical extent are consistent with *Newman et al.* [1996] who observed shallow intrusions at midlatitudes in the lower stratosphere, as well as with the studies by *Orsolini* [1995], *Orsolini et al.*

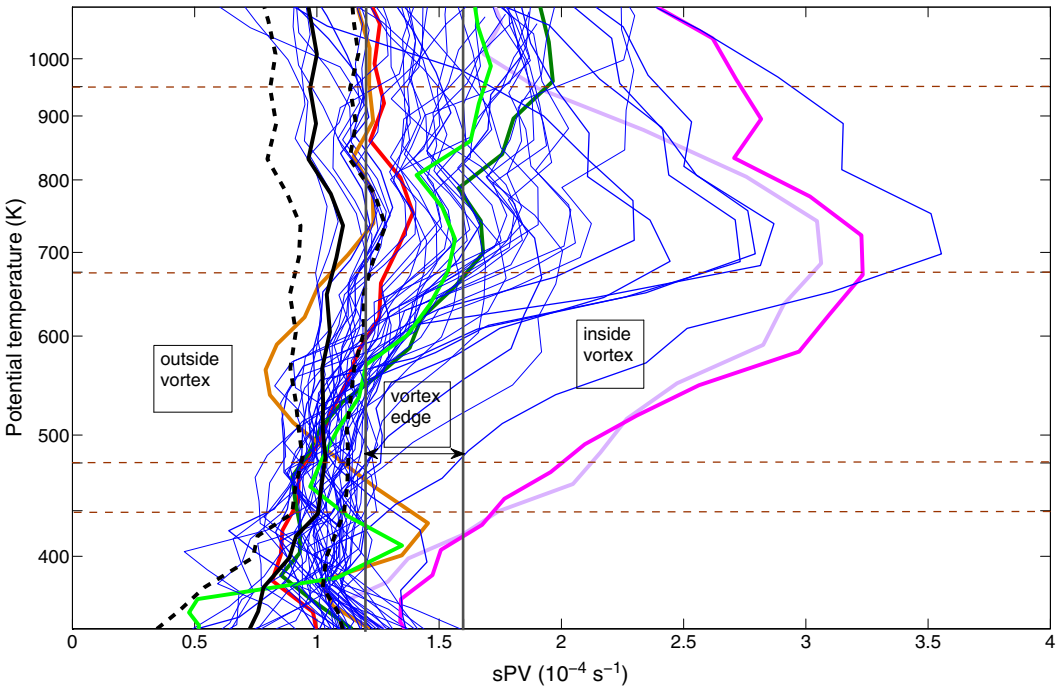

Figure 12. Scaled potential vorticity over Toronto during the 53 polar intrusion events derived from MERRA (blue and colored lines). The grey vertical lines indicate the outer and inner polar vortex edges. The horizontal dashed lines are the four vertical levels at which sPV was sampled in the time series. The thick black line and dashed black lines are the mean sPV profile from all nonintrusion days and its standard deviation, respectively. The colored lines are sPV profiles from specific days that were discussed in sections 4.2 and 4.4: mauve = 20 January 2003, red = 14 May 2003, dark green = 14 December 2004, orange = 3 March 2005, pink = 16 January 2009, and light green = 27 October 2010.

[1997], and *Schoeberl and Newman* [1995] who observed and modeled both shallow and deep polar vortex filaments throughout the stratosphere.

5. Conclusions

[57] We have presented the TAO and CARE ground-based FTIR time series of stratospheric HF, HCl, O_3, and N_2O partial columns measured from January 2002 to March 2013 and have used these results, along with the sPV analysis, to identify 53 polar intrusion events over the densely populated Toronto area. All 11 years had at least 2 days with a polar intrusion event detected in enhanced HF columns, with four events per year being the average. Most of the events were detected in the late fall, winter, or early spring, when the polar vortex was formed or distorted, rapidly changing, and frequently shedding filaments. These conditions commonly occur throughout Arctic fall and winter [e.g., *Manney et al.*, 2000]. To our knowledge, this is the first study to use ground-based FTIR column measurements to identify multiple polar intrusions over the course of a decade over a particular midlatitude region and to examine the impact of intrusions on the stratospheric columns of four different trace gases.

[58] FTIR measurements of HF columns were useful for detecting polar vortex intrusions; the HF stratospheric columns were enhanced during 100% of the lower stratosphere (435 K and 475 K) polar vortex (sPV > $1.6 \times 10^{-4} s^{-1}$) overpasses. When the upper stratosphere (675 K and 950 K) polar vortex intrusions are also included, 40% of HF stratospheric columns were enhanced, as the upper stratosphere contributes less overall to the HF columns. However, 40% is still a significant amount detected by HF column measurements. When the polar vortex *edge* (sPV > $1.2 \times 10^{-4} s^{-1}$) overpasses are also included, the percentage drops to 30%(25%) for the lower (upper) stratosphere events.

[59] Most of the late fall, winter, and early spring variability in the TAO HF time series (Figure 7) can be explained by transient polar intrusion events, although the magnitude of the effect varies from year to year. The effect on the O_3 time series (FTIR and OSIRIS) is irregular (Figure 7, Table 3); most of the time, there is a small increase in O_3 during an event, even when there is O_3 depletion inside the vortex. The vortex filaments often do not share the O_3-depleted state of the vortex (e.g., the unprecedented O_3 loss in 2011 did not cause a decrease in Toronto O_3 columns). Based on our results and the *Marchand et al.* [2003] study, O_3 depletion over Toronto is more likely to occur during a vortex excursion, and these are rarer than filaments.

[60] The vertical profiles of sPV (Figure 12) show that the intrusions can occur at varying altitudes and span various vertical ranges. While the FTIR retrievals cannot resolve those features, the sensitivity in the 12–50 km range is sufficient to see variability in the stratospheric columns caused by these polar intrusion events, including mid-to-upper stratospheric events, which are not measurable with sondes, lidar, aircraft, and in situ instruments.

[61] FTIR spectroscopy is capable of measuring numerous polar vortex tracers and stratospheric gases important for O_3 chemistry over long periods. There are 14 NDACC

sites north of 40°N; many of which have been taking observations for more than a decade (e.g., http://www.acd.ucar.edu/irwg/). Based on the results of this study, these data sets should also provide evidence of polar intrusion events and afford an opportunity to study the accuracy of their representation in models.

[62] **Acknowledgments.** Funding for this work was provided by the Natural Sciences and Engineering Research Council of Canada, the Canadian Space Agency (CSA), and Environment Canada. The TAO measurements have been supported in the past by the Canadian Foundation for Climate and Atmospheric Sciences, ABB Bomem, the Canada Foundation for Innovation, the Ontario Research and Development Challenge Fund, the Premier's Research Excellence Award, and the University of Toronto. We also wish to thank the many students, postdocs, and interns who have contributed to TAO data acquisition since 2001.

[63] The CARE DA8 was operated by Environment Canada. OSIRIS is onboard Odin, a Swedish-led satellite project funded jointly by Sweden (SNSB), Canada (CSA), Finland (TEKES), and France (CNES) and supported since 2007 by the third party mission program of the European Space Agency. EP/TOMS and OMI maps were prepared by the Ozone Processing Team of NASA/Goddard Space Flight Center. The MERRA data used in this effort were acquired as part of the activities of NASA's Science Mission Directorate and are archived and distributed by the Goddard Earth Sciences Data and Information Services Center. The authors acknowledge Ether, the French data center for atmospheric chemistry, created and codirected by the Centre National d'Études Spatiales (CNES) and the National Institute of Sciences of the Universe (INSU-CNRS) for the provision of MIMOSA data. We thank Susan E. Strahan (NASA Goddard Earth Science and Technology Center) for the GMI model output. Work at the Jet Propulsion Laboratory, California Institute of Technology was done under contract with the National Aeronautic and Space Administration.

References

Adams, C., et al. (2012), Severe 2011 ozone depletion assessed with 11 years of ozone, NO_2, and OClO measurements at 80°N, *Geophys. Res. Lett.*, *39*, L05806, doi:10.1029/2011GL050478.

Adams, C., et al. (2013a), Characterization of Odin-OSIRIS ozone profiles with the SAGE II dataset, *Atmos. Meas. Tech.*, *6*, 1447–1459, doi:10.5194/amt-6-1447-2013.

Adams, C., A. E. Bourassa, V. Sofieva, L. Froidevaux, C. A. McLinden, D. Hubert, J.-C. Lambert, C. E. Sioris, and D. A. Degenstein (2013b), Assessment of Odin-OSIRIS ozone measurements from 2001 to the present using MLS, GOMOS, and ozone sondes, *Atmos. Meas. Tech. Discuss.*, *6*, 3819–3857, doi:10.5194/amtd-6-3819-2013.

Andrews, D. G., J. R. Holton, and C. B. Leovy (1987), *Middle Atmosphere Dynamics*, Academic Press, London.

Balis, D., et al. (2011), Observed and modelled record ozone decline over the Arctic during winter/spring, *Geophys. Res. Lett.*, *38*, L23801, doi:10.1029/2011GL049259.

Brasseur, G. P., J. J. Orlando, and G. S. Tyndall (1999), *Atmospheric Chemistry and Global Change*, Oxford Univ. Press, New York.

Butchart, N., and E. E. Remsberg (1986), The area of the stratospheric polar vortex as a diagnostic for tracer transport on an isentropic surface, *J. Atmos. Sci.*, *43*, 1319–1339.

Chipperfield, M. P., et al. (1997), On the use of HF as a reference for the comparison of stratospheric observations and models, *J. Geophys. Res.*, *102*(D11), 12,901–12,919, doi:10.1029/96JD03964.

Christensen, T., et al. (2005), Vortex-averaged Arctic ozone depletion in the winter 2002/2003, *Atmos. Chem. Phys.*, *5*, 131–138, doi:10.5194/acp-5-131-2005.

Coffey, M. T., et al. (2008), Airborne Fourier transform spectrometer observations in support of EOS Aura validation, *J. Geophys. Res.*, *113*, D16S42, doi:10.1029/2007JD008833.

Degenstein, D. A., A. E. Bourassa, C. Z. Roth, and E. J. Llewellyn (2009), Limb scatter ozone retrieval from 10 to 60 km using a multiplicative algebraic reconstruction technique, *Atmos. Chem. Phys.*, *9*, 6521–6529, doi:10.5194/acp-9-6521-2009.

Duchatelet, P., et al. (2009), An approach to retrieve information on the carbonyl fluoride (COF_2) vertical distributions above Jungfraujoch by FTIR multi-spectrum multi-window fitting, *Atmos. Chem. Phys.*, *9*, 9027–9042, doi:10.5194/acp-9-9027-2009.

Duncan, B. N., S. E. Strahan, Y. Yoshida, S. D. Steenrod, and N. Livesey (2007), Model study of the cross-tropopause transport of biomass burning pollution, *Atmos. Chem. Phys.*, *7*, 3713–3736, doi:10.5194/acp-7-3713-2007.

Dunkerton, T. J., and D. P. Delisi (1986), Evolution of potential vorticity in the winter stratosphere of January–February 1979, *J. Geophys. Res.*, *91*(D1), 1199–1208, doi:10.1029/JD091iD01p01199.

Durry, G., and A. Hauchecorne (2005), Evidence for long-lived polar vortex air in the mid-latitude summer stratosphere from in situ laser diode CH4 and H2O measurements, *Atmos. Chem. Phys.*, *5*, 1467–1472, doi:10.5194/acp-5-1467-2005.

Eyring, V., et al. (2007), Multimodel projections of stratospheric ozone in the 21st century, *J. Geophys. Res.*, *112*, D16303, doi:10.1029/2006JD008332.

Fairlie, T. D. A., R. B. Pierce, W. L. Grose, G. Lingenfelser, M. Loewenstein, and J. R. Podolske (1997), Lagrangian forecasting during ASHOE/MAESA: Analysis of predictive skill for analyzed and reverse-domain-filled potential vorticity, *J. Geophys. Res.*, *102*(D11), 13,169–13,182, doi:10.1029/96JD03507.

Godin, S., M. Marchand, A. Hauchecorne, and F. Lefèvre (2002), Influence of Arctic polar ozone depletion on lower stratospheric ozone amounts at Haute-Provence Observatory (43.92°N, 5.71°E), *J. Geophys. Res.*, *107*(D20), 8272, doi:10.1029/2001JD000516.

Harvey, V. L., R. B. Pierce, T. D. Fairlie, and M. H. Hitchman (2002), A climatology of stratospheric polar vortices and anticyclones, *J. Geophys. Res.*, *107*(D20), 4442, doi:10.1029/2001JD001471.

Hauchecorne, A., S. Godin, M. Marchand, B. Heese, and C. Souprayen (2002), Quantification of the transport of chemical constituents from the polar vortex to midlatitudes in the lower stratosphere using the high-resolution advection model MIMOSA and effective diffusivity, *J. Geophys. Res.*, *107*(D20), 8289, doi:10.1029/2001JD000491.

Hoskins, B. J., M. E. McIntyre, and A. W. Robertson (1985), On the use and significance of isentropic potential vorticity maps, *Q. J. R. Meteorol. Soc.*, *111*, 877–946, doi:10.1002/qj.49711147002.

Jayanarayanan, K., A. Kleinbohl, M. Sinnhuber, H. Bremer, H. Kullmann, J. Notholt, S. Godin-Beekmann, O. Tripathi, and G. Nikulin (2011), Arctic ozone depletion in 20020–2003 measured by ASUR and comparison with POAM observations, *J. Geophys. Res.*, *116*, D22305, doi:10.1029/2011JD016020.

Kagawa, A., Y. Kasai, N. B. Jones, M. Yamamori, K. Seki, F. Murcray, Y. Murayama, K. Mizutani, and T. Itabe (2007), Characteristics and error estimation of stratospheric ozone and ozone-related species over Poker Flat (65°N, 147°W), Alaska observed by a ground-based FTIR spectrometer from 2001 to 2003, *Atmos. Chem. Phys.*, *7*, 3791–3810, doi:10.5194/acp-7-3791-2007.

Keckhut, P., C. David, M. Marchand, S. Bekki, J. Jumelet, A. Hauchecorne, and M. Höpfner (2007), Observation of polar stratospheric clouds down to the Mediterranean coast, *Atmos. Chem. Phys.*, *7*, 5275–5281, doi:10.5194/acp-7-5275-2007.

Konopka, P., J.-U. Grooß, S. Bausch, R. Müller, D. S. McKenna, O. Morgenstern, and Y. Orsolini (2003), Dynamics and chemistry of vortex remnants in late Arctic spring 1997 and 2000: Simulations with the Chemical Lagrangian Model of the Stratosphere (CLaMS), *Atmos. Chem. Phys.*, *3*, 839–849, doi:10.5194/acp-3-839-2003.

Labitzke, K., and M. Kunze (2009), On the remarkable Arctic winter in 2008/2009, *J. Geophys. Res.*, *114*, D00I02, doi:10.1029/2009JD012273.

Leovy, C. B., C.-R. Sun, M. Hitchman, E. E. Remsburg, J. M. Russell III, L. L. Gordley, J. C. Gille, and L. V. Lyjak (1985), Transport of ozone in the middle stratosphere: Evidence for planetary wave breaking, *J. Atmos. Sci.*, *42*, 230–244, doi:10.1175/1520-0469(1985)042<0230:TOOITM>2.0.CO;2.

Lindenmaier, R., R. Batchelor, K. Strong, H. Fast, F. Goutail, F. Kolonjari, C. T. McElroy, R. Mittermaier, and K. Walker (2010), An evaluation of infrared microwindows for ozone retrievals using the Eureka Bruker 125HR Fourier transform spectrometer, *J. Quant. Spectrosc. Radiat. Transfer.*, *111*, 569–585, doi:10.1016/j.jqsrt.2009.10.013.

Lindenmaier, R. et al. (2012), Unusually low ozone, HCl, and HNO_3 column measurements at Eureka, Canada during winter/spring 2011, *Atmos. Chem. Phys.*, *12*, 3821–3835, doi:10.5194/acp-12-3821-2012.

Llewellyn, E., et al. (2004), The OSIRIS instrument on the Odin spacecraft, *Can. J. Phys.*, *82*, 411–422, doi:10.1139/p04-005.

Manney, G. L., R. W. Zurek, A. O'Neill, and R. Swinbank (1994), On the motion of air through the stratospheric polar vortex, *J. Atmos. Sci.*, *51*, 2973–2994, doi:10.1175/1520-0469(1994)051<2973:OTMOAT>2.0.CO;2.

Manney, G. L., J. C. Bird, D. P. Donovan, T. J. Duck, J. A. Whiteway, S. R. Pal, and A. I. Carswell (1998), Modeling ozone laminae in ground-based Arctic wintertime observations using trajectory calculations and satellite data, *J. Geophys. Res.*, *103*(D5), 5797–5814, doi:10.1029/97JD03449.

Manney, G. L., H. A. Michelsen, F. W. Irion, M. R. Gunson, G. C. Toon, and A. E. Roche (2000), Lamination and polar vortex development in fall from ATMOS long-lived trace gases observed during November 1994, *J. Geophys. Res.*, *105*(D23), 29,023–29,038, doi:10.1029/2000JD900428.

Manney, G. L., et al. (2007), Solar occultation satellite data and derived meteorological products: Sampling issues and comparisons with Aura Microwave Limb Sounder, *J. Geophys. Res.*, *112*, D24550, doi:10.1029/2007JD008709.

Manney, G. L., M. J. Schwartz, K. Krüger, M. L. Santee, S. Pawson, J. N. Lee, W. H. Daffer, R. A. Fuller, and N. J. Livesey (2009), Aura Microwave Limb Sounder observations of dynamics and transport during the record-breaking 2009 Arctic stratospheric major warming, *Geophys. Res. Lett.*, *36*, L12815, doi:10.1029/2009GL038586.

Manney, G. L., et al. (2011), Unprecedented Arctic ozone loss in 2011, *Nature*, *478*, 469–475, doi:10.1038/nature10556.

Marchand, M., S. Godin, A. Hauchecorne, F. Lefèvre, S. Bekki, and M. Chipperfield (2003), Influence of polar ozone loss on northern midlatitude regions estimated by a high-resolution chemistry transport model during winter 1999/2000, *J. Geophys. Res.*, *108*(D5), 8326, doi:10.1029/2001JD000906.

McIntyre, M. E., and T. N. Palmer (1984), The "surf zone" in the stratosphere, *J. Atmos. Terr. Phys.*, *9*, 825–849.

Mellqvist, J., B. Galle, T. Blumenstock, F. Hase, D. Yashcov, J. Notholt, B. Sen, J.-F. Blavier, G. C. Toon, and M. P. Chipperfield (2002), Ground-based FTIR observations of chlorine activation and ozone depletion inside the Arctic vortex during the winter of 1999/2000, *J. Geophys. Res.*, *107*(D20), doi:10.1029/2001JD001080.

Millard, G. A., A. M. Lee, and J. A. Pyle (2003), A model study of the connection between polar and midlatitude ozone loss in the Northern Hemisphere lower stratosphere, *J. Geophys. Res.*, *108*(D5), 8323, doi:10.1029/2001JD000899.

Murtagh, D., et al. (2002), An overview of the Odin atmospheric mission, *Can. J. Phys.*, *80*, 309–319, doi:10.1139/p01-157.

Nash, E. R., P. A. Newman, J. E. Rosenfield, and M. R. Schoeberl (1996), An objective determination of the polar vortex using Ertel's potential vorticity, *J. Geophys. Res.*, *101*(D5), 9471–9478, doi:10.1029/96JD00066.

Newman, P. A., et al. (1996), Measurements of polar vortex air in midlatitudes, *J. Geophys. Res.*, *101*(D8), 12,879–12,891, doi:10.1029/95JD03387.

Orsolini, Y. J. (1995), On the formation of ozone laminae at the edge of the Arctic polar vortex, *Q. J. R. Meteorol. Soc.*, *121*, 1923–1941, doi:10.1002/qj.49712152808.

Orsolini, Y. J., G. Hansen, U. Hoppe, G. L. Manney, and K. Fricke (1997), Dynamical modelling of wintertime Lidar observations in the Arctic: Ozone laminae and ozone depletion, *Q. J. R. Meteorol. Soc.*, *123*, 785–800, doi:10.1002/qj.49712353913.

Orsolini, Y. J., G. L. Manney, A. Engel, J. Ovarlez, C. Claud, and L. Coy (1998), Layering in stratospheric profiles of long-lived trace species: Balloon-borne observations and modeling, *J. Geophys. Res.*, *103*(D5), 5815–5825, doi:10.1029/97JD03131.

Orsolini, Y. J., and W. B. Grant (2000), Seasonal formation of nitrous oxide laminae in the mid and low latitude stratosphere, *Geophys. Res. Lett.*, *27*(D8), 1119–1122, doi:10.1029/1999GL011172.

Orsolini, Y. J., G. Hansen, G. L. Manney, N. J. Livesey, and U.-P. Hoppe (2001), Lagrangian reconstruction of ozone column and profile at the Arctic Lidar Observatory for Middle Atmosphere Research (ALOMAR) throughout winter and spring 1997–98, *J. Geophys. Res.*, *106*(D9), 10,011–10,021, doi:10.1029/2000JD900659.

Pierce, R. B., and T. D. A. Fairlie (1993), Chaotic advection in the stratosphere: Implications for the dispersal of chemically perturbed air from the polar vortex, *J. Geophys. Res.*, *98*(D10), 18,589–18,595, doi:10.1029/93JD01619.

Pougatchev, N., B. Connor, and C. Rinsland (1995), Infrared measurements of the ozone vertical distribution above Kitt Peak, *J. Geophys. Res.*, *100*(D8), 16,689–16,697, doi:10.1029/95JD01296.

Rienecker, M. M., et al. (2011), MERRA: NASA's Modern-Era retrospective analysis for research and applications, *J. Clim.*, *24*, 3624–3628.

Rinsland, C. P., et al. (1998), Nothern and southern hemisphere ground-based infrared spectroscopic measurements of tropospheric carbon monoxide and ethane, *J. Geophys. Res.*, *103*(D21), 28,197–28,217, doi:10.1029/98JD02515.

Rodgers, C. D. (2000), *Inverse Methods For Atmospheric Sounding: Theory and Practice (Series on Atmospheric, Oceanic and Planetary Physics)*, vol. 2, World Scientific Publishing Co. Pte. Ltd., New Jersey.

Rösevall, J. D., D. P. Murtagh, and J. Urban (2007), Ozone depletion in the 2006/2007 Arctic winter, *Geophys. Res. Lett.*, *34*, L21809, doi:10.1029/2007GL030620.

Rösevall, J. D., D. P. Murtagh, J. Urban, W. Feng, P. Eriksson, and S. Brohede (2008), A study of ozone depletion in the 2004/2005 Arctic winter based on data from Odin/SMR and Aura/MLS, *J. Geophys. Res.*, *113*, D13301, doi:10.1029/2007JD009560.

Rothman, L. S., et al. (2009), The HITRAN 2008 molecular spectroscopic database, *J. Quant. Spectrosc. Radiat. Transfer.*, *110*, 533–572.

Schoeberl, M. R., L. R. Lait, P. A. Newman, and J. E. Rosenfield (1992), The structure of the polar vortex, *J. Geophys. Res.*, *97*(D8), 7859–7882, doi:10.1029/91JD02168.

Schoeberl, M. R., M. Luo, and J. E. Rosenfield (1995), An analysis of the Antarctic Halogen Occultation Experiment trace gas observations, *J. Geophys. Res.*, *100*(D3), 5159–5172, doi:10.1029/94JD02749.

Schoeberl, M. R., and P. A. Newman (1995), A multiple-level trajectory analysis of vortex filaments, *J. Geophys. Res.*, *100*(D12), 25,801–25,815, doi:10.1029/95JD02414.

Singleton, C. S., C. E. Randall, M. P. Chipperfield, S. Davies, W. Feng, R. M. Bevilacqua, K. W. Hoppel, M. D. Fromm, G. L. Manney, and V. L. Harvey (2005), 2002-2003 Arctic ozone loss deduced from POAM III satellite observations and the SLIMCAT chemical transport model, *Atmos. Chem. Phys.*, *5*, 597–609, doi:10.5194/acp-5-597-2005.

Sonkaew, T., C. von Savigny, K.-U. Eichmann, M. Weber, A. Rozanov, H. Bovensmann, and J. P. Burrows (2011), Chemical ozone loss in Arctic and Antarctic polar winter/spring season derived from SCIAMACHY limb measurements 2002–2009, *Atmos. Chem. Phys. Discuss.*, *11*, 6555–6599, doi:10.5194/acpd-11-6555-2011.

Søvde, O. A., Y. J. Orsolini, D. R. Jackson, F. Stordal, I. S. A. Isaksen, and B. Rognerud (2011), Estimation of Arctic O_3 loss during winter 2006/2007 using data assimilation and comparison with a chemical transport model, *Q. J. R. Meteorol. Soc.*, *137*, 118–128, doi:10.1002/qj.740.

Strahan, S. E., B. N. Duncan, and P. Hoor (2007), Observationally derived transport diagnostics for the lowermost stratosphere and their application to the GMI chemistry and transport model, *Atmos. Chem. Phys.*, *7*, 2435–2445, doi:10.5194/acp-7-2435-2007.

Sutton, R. T., H. Maclean, R. Swinbank, A. O'Neill, and F. W. Taylor (1994), High-resolution stratospheric tracer fields estimated from satellite observations using Lagrangian trajectory calculations, *J. Atmos. Sci.*, *51*, 2995–3005.

Taylor, J. R., K. Strong, C. A. McLinden, D. A. Degenstein, and C. S. Haley (2007), Comparison of OSIRIS stratospheric NO_2 and O_3 measurements with ground-based Fourier transform spectrometer measurements at the Toronto Atmospheric Observatory, *Can. J. Phys.*, *85*, 1301–1316, doi:10.1139/P07-144.

Taylor, J. R., D. Wunch, C. Midwinter, A. Wiacek, J. R. Drummond, and K. Strong (2008), An extended intercomparison of simultaneous ground-based Fourier transform infrared spectrometer measurements at the Toronto Atmospheric Observatory, *J. Quant. Spectrosc. Radiat. Transfer.*, *109*, 2244–2260, doi:10.1016/j.jqsrt.2008.03.011.

Toon, G. C., J.-F. Blavier, B. Sen, R. J. Salawitch, G. B. Osterman, J. Notholt, M. Rex, C. T. McElroy, and J. M. Russell III (1999), Ground-based observations of Arctic O_3 loss during spring and summer 1997, *J. Geophys. Res.*, *104*(D21), 26,497–26,510, doi:10.1029/1999JD900745.

Tripathi, O. P., T. Leblanc, I. S. McDermid, F. Lefèvre, M. Marchand, and A. Hauchecorne (2006), Forecast, measurement, and modeling of an unprecedented polar ozone filament event over Mauna Loa Observatory, Hawaii, *J. Geophys. Res.*, *111*, D20308, doi:10.1029/2006JD007177.

Vigouroux, C., et al. (2008), Evaluation of tropospheric and stratospheric ozone trends over Western Europe from ground-based FTIR network observations, *Atmos. Chem. Phys.*, *8*, 6865–6886, doi:10.5194/acp-8-6865-2008.

Waugh, D. W., et al. (1994), Transport out of the lower stratospheric Arctic vortex by Rossby wave breaking, *J. Geophys. Res.*, *99*(D1), 1071–1088, doi:10.1029/93JD02556.

Wiacek, A. (2006), First trace gas measurements using Fourier transform infrared solar absoption spectroscopy at the University of Toronto Atmospheric Observatory, PhD thesis, Department of Physics, University of Toronto.

Wiacek, A., J. R. Taylor, K. Strong, R. Saari, and T. E. Kerzenmacher (2007), Ground-based solar absorption FTIR spectroscopy: Characterization of retrievals and first results from a novel optical design instrument at a new NDACC complementary station, *J. Atmos. Oceanic Tech.*, *24*, 432–448, doi:10.1175/JTRCH1962.1.

WMO, (2007), World Meteorological Organization Scientific Assessment of Ozone Depletion: 2006, *WMO Global Ozone Research and Monitoring Project-Report 50*, Geneva, Switzerland.

Wunch, D., J. R. Taylor, D. Fu, P. F. Bernath, J. R. Drummond, C. Midwinter, K. Strong, and K. A. Walker (2007), Simultaneous ground-based observations of O_3, HCl, N_2O, and CH_4 over Toronto, Canada by three Fourier transform spectrometers with different resolutions, *Atmos. Chem. Phys.*, *7*, 1275–1292, doi:10.5194/acp-7-1275-2007.